Interpretation of the Nitrogen isotopic composition of Precambrian sedimentary rocks: assumptions and perspectives

M. Ader[a], C. Thomazo[b], P. Sansjofre[c], V. Busigny[a],

D. Papineau[d], R. Laffont[b], P. Cartigny[a], G.P. Halverson[e]

[a] Institut de Physique du Globe de Paris, Sorbonne Paris Cité, University Paris Diderot, UMR 7154 CNRS, 1 rue Jussieu, 75238 Paris, France

[b] Biogéosciences, Université de Bourgogne Franche-Comté, UMR6282 CNRS, 21000 Dijon, France.

[c] IUEM, Laboratoire Domaines Océaniques, Université de Bretagne Occidentale, UMR 6538, 29820 Plouzané, France

[d] London Centre for Nanotechnology and Department of Earth Sciences, University College London, 17-19 Gordon Street, WC1H 0AH, United Kingdom

[e] Department of Earth and Planetary Sciences/Geotop, McGill University, 3450 University Street, Montréal, QC, Canada H3A 0E8.

Keywords: Nitrogen isotopes; Precambrian; Nitrogen biogeochemical cycle; Ocean oxygenation

Abstract

With the surge of interest in understanding the evolution of environments and ecosystems on the early Earth, many proxies are being applied to ancient sedimentary rocks. The isotope composition of nitrogen recorded in sedimentary rocks ($\delta^{15}N_{sed}$) is one of these proxies. Nitrogen isotopes are now routinely used as a tracer of the global and regional marine N-biogeochemical cycle during the Cenozoic and are increasingly being applied to the ancient rock record, including the Precambrian. The objectives of this review are (i) to articulate guidelines for using $\delta^{15}N_{sed}$ as a proxy for the past marine global N-biogeochemical cycle with an emphasis on the Precambrian and (ii) to develop a broad framework for interpreting the Precambrian $\delta^{15}N_{sed}$ record. Based on the isotopic pattern displayed by the present day N-biogeochemical cycle, significant $\delta^{15}N_{sed}$ spatial variability is expected for most of the ocean redox structures envisaged for the Precambrian. Furthermore, fundamentally different N-cycling processes may give rise to only subtly different $\delta^{15}N_{sed}$ signatures, which themselves may be masked or accentuated by post-depositional processes. Consequently, $\delta^{15}N_{sed}$ profiles from individual basins alone are insufficient for inferring behavior of the global nitrogen cycle. Rather, $\delta^{15}N_{sed}$ distributions based on data from multiple basins are essential. Furthermore, in order to interpret $\delta^{15}N_{sed}$ data from Precambrian sedimentary rocks with more confidence, several avenues of focused research are required. The effects of diagenesis and metamorphism and their manifestation in the $\delta^{15}N$ compositions of both bulk and kerogen records need to be better understood. Much more data are required in order to apply statistical approaches to interpreting $\delta^{15}N_{sed}$ variability within given geological time intervals. Finally, numerical modeling of the $\delta^{15}N_{sed}$ distributions expected from different redox scenarios envisaged for the Precambrian environment is necessary to establish a predictive template for interpreting the ancient nitrogen isotope record. In spite of the intrinsic complexity of the

$\delta^{15}N_{sed}$ proxy and the great deal of work still required to realize its full potential, the available Precambrian $\delta^{15}N_{sed}$ record shows several intuitive features within the context of the inferred evolution of the marine N-biogeochemical cycle. The $\delta^{15}N_{sed}$ distributions are roughly similar in shape and amplitude to that of the present ocean, with a change in mode from +1 to +3‰ at ca. 2.7 Ga and transient excursions to ^{15}N-enriched values at 2.7 and 1.9 Ga. Fundamental shifts in global marine N-cycling, perhaps related to stepwise oxygenation of the surface environment, are inferred, highlighting the potential of nitrogen isotopes to reveal clues about the evolution of early Earth.

1. Introduction

Characterizing the evolution of the marine nitrogen biogeochemical cycle through time and identifying its driving factors is critical to fully understanding the evolution of the Earth's surface environments for at least two interconnected reasons. First, nitrogen (N) is present in the ocean mostly as the bioavailable species nitrate (NO_3^-), nitrite (NO_2^-), ammonium (NH_4^+) and dissolved organic nitrogen (DON). Because N is one of the major constituents of life (with C/N ratio between 4 and 10 for the oceanic phytoplankton), these bioavailable species exert a strong control on primary productivity, and hence on the biogeochemical C cycle (e.g., Tyrell, 1999; Falkoswki, 1997; Gruber and Galloway, 2008; Canfield et al., 2010). Second, N is also present in Earth's atmosphere, mostly as di-nitrogen (N_2), which is by far the most abundant gas in the atmosphere (78.06% by volume today), but also in trace amounts as N_2O, NH_3 and other NO_x species, whose abundances are in part controlled by the marine N-biogeochemical cycle. Both the N_2 partial pressure and the abundance of these trace

greenhouse gas species in the atmosphere influence the global climate linking it to the N-cycle (Buik, 2007; Goldblatt et al., 2009; Roberson et al., 2011; Thunell and Kepple, 2004).

An obvious approach to reconstructing the evolution of the marine N-biogeochemical cycle, and hence its role in shaping ancient surface environments, is to interrogate the isotope composition of N preserved in sedimentary rocks ($\delta^{15}N_{sed}$). As for any geochemical tracer, the ability to extract meaningful paleoenvironmental information from N isotopes requires several conditions be met. First, reliable (precise and reproducible) $\delta^{15}N_{sed}$ measurements are necessary. Second, post-depositional processes must not have significantly modified $\delta^{15}N_{sed}$ values. Finally, and perhaps most challengingly, $\delta^{15}N_{sed}$ values must be related to processes in the biogeochemical nitrogen cycle.

In the last 50 years, major progress has been made in understanding controls on N isotope signatures of nitrate, particulate organic matter, surface sediments (e.g. Somes et al., 2010; Tesdal et al., 2013; Thunell et al., 2004) and early diagenetic processes (e.g. Robinson et al., 2012) in modern environments. Although many uncertainties remain, these studies have yielded several guidelines to the interpretation of N isotopes in modern sediments: (i) in anoxic basins and continental platforms, $\delta^{15}N$ of primary producers is transmitted to the sediment, (ii) the $\delta^{15}N$ value of primary producers typically reflects the $\delta^{15}N$ of assimilated N, and (iii) the speciation and $\delta^{15}N$ values of bio-available N in the surface ocean mostly depend on the dominant processes in the N cycle in the ocean (and hence on ocean redox structure). Available data indicate that $\delta^{15}N_{sed}$ signatures are faithful proxies for biogeochemical processes in the marine realm at least in the recent past (e.g. Galbraith et al., 2008).

$\delta^{15}N$ analyses of ancient sedimentary rocks began in earnest in the 1980's (e.g. Hayes et al., 1983; Zang, 1988). In the case of Precambrian rocks, the field developed slowly for the subsequent 30 years mostly due to the technical difficulty of making measurements in N-poor

samples. Two other issues have also historically impeded the application of N isotopes to the Precambrian: uncertainties about the preservation of a primary $\delta^{15}N$ signal in often metamorphosed samples and limited understanding of how the modern N cycle and its isotopic transcription into sedimentary organic matter can be applied to interpreting Precambrian datasets. However, recent technical advances have opened the door to rapid and reliable analysis of minute quantities of N, sometimes coupled with simultaneous analyses of organic carbon (e.g. Polissar et al., 2008). Application of the proxy has thus accelerated in the past five years. Numerous N isotopes studies in Precambrian sedimentary rocks have been performed with two broad objectives: (i) reconstructing the N-biogeochemical cycle and its relations to water column redox structure of Precambrian marine environments (e.g. Papineau et al., 2009; Busigny et al., 2013; Stüeken et al., 2013; Ader et al., 2014) and (ii) documenting the Precambrian evolution and radiation of organisms performing the main metabolic pathways of the N cycle, such as NH_4^+ oxidation (Thomazo et al., 2011), denitrification (Beaumont and Robert, 1999; Garvin et al., 2009; Godfrey and Falkowski, 2009) and N_2-fixation (Stüeken et al., 2015a).

The application of N isotope systematics is bound to increase with a surge in interest in the coevolution of Precambrian environments and life, which is driving multi-proxy approaches to extract increasingly nuanced information about ancient nutrient cycling and metabolic pathways. In light of significant recent progress, it is timely to revisit and fortify the underpinnings of the nitrogen isotope interpretational framework as applied to the Precambrian. To this end, rather than reviewing how $\delta^{15}N_{sed}$ data have been interpreted in terms of the Precambrian marine N-biogeochemical cycle (e.g., Pinti and Hashizume, 2011; Thomazo et al., 2009; Thomazo and Papineau, 2013), our objectives are (i) to evaluate our confidence in applying the N isotope system to very old rocks and (ii) to identify future

directions of research to progress the application of the N isotope system to unraveling Precambrian environments and biogeochemical processes.

We have subdivided this paper into six sections. The first four sections are dedicated to reviewing the main conditions required to extract meaningful information from N isotopes and to discuss their applicability to the Precambrian (Fig. 1): (i) That analytically reliable $\delta^{15}N_{sed}$ measurements can be made; (ii) That absence of post-depositional modification of $\delta^{15}N$ value of surface sediments after deposition can be demonstrated or inferred; (iii) That $\delta^{15}N$ values of surface sediments can be assumed to be systematically related to the composition of primary producers; and (iv) That $\delta^{15}N$ values of primary producers reflect speciation and isotope composition of the N assimilated in the photic zone. The fifth section explores the extent to which different possible modes of global marine N-cycling should translate into distinct and recognizable $\delta^{15}N$ signatures based on conceptual models of N-cycling in oceans with different redox structure. The last section uses an updated compilation of published Precambrian $\delta^{15}N_{sed}$ data as a platform to identify and interpret the main features of the Precambrian N isotope record.

2. $\delta^{15}N$ measurements of Precambrian sedimentary rocks

Precambrian sedimentary rocks commonly contain little total N due to their typically low organic matter content and their long and often complex post-depositional history, (supplementary Table 1 and references therein). These low N-contents present an analytical challenge, which until recently strongly limited the acquisition of N isotope data. Isotopic measurements on Precambrian rocks are mostly bulk analyses ($\delta^{15}N_{bulk}$), in which the

141 measured N includes both organically bound N and nitrogen incorporated in minerals,
142 typically in the form of NH_4^+ bound within clays and other silicate minerals. But N isotopes
143 have also been measured in kerogens ($\delta^{15}N_{ker}$), graphite, mineral separates ($\delta^{15}N_{NH4}$) and fluid
144 inclusions ($\delta^{15}N_{N2}$). All measurements are made on gaseous N_2 via gas-source isotope-ratio
145 mass spectrometry (IRMS), but several methods and apparatuses have been used to oxidize
146 organic-N and/or silicate bound NH_4^+ from ancient sedimentary rocks into N_2 gas, which can
147 then be measured by IRMS.

148 In the classical method, N_2 is produced offline from the sample material through sealed-tube
149 (Dumas) combustion, purified in a vacuum line, and introduced via dual-inlet into a dynamic-
150 vacuum IRMS. This method is the most precise as it yields errors of less than ±0.3‰ (2σ),
151 but it can only be performed for N_2 quantities higher than 2 μmole, limiting its use to samples
152 containing more than 200 ppm N (for sealed tubes loaded with 200 mg of sample) (e.g. Ader
153 et al., 2014). The first $\delta^{15}N$ data for Precambrian rocks were acquired on kerogen extracts by
154 this technique (Hayes et al., 1983; Beaumont and Robert, 1999), albeit with a much poorer
155 precision than the 0.3‰ (2σ), that can be achieved by modern techniques.

156 In the static method, N_2 is produced by either off-line sealed-tube combustion or on-line step
157 heating and then purified in an ultra-high vacuum line with direct introduction into a static-
158 vacuum IRMS (e.g., Sano and Pillinger 1990; Wright et al., 1998; Boyd et al., 1993; Busigny
159 et al., 2005). This approach allows $\delta^{15}N$ analyses on samples containing only a few ppm N.
160 Only a handful of laboratories have produced $\delta^{15}N$ data using this technique. The Open
161 University (e.g., Sephton et al., 2003), CRPG in Nancy (France) (e.g. Marty et al., 2013) and
162 Osaka University (Japan) (e.g., Pinti et al., 2001; 2007; 2009) have employed an on-line step
163 heating system. IPGP (France) has used both an on-line step heating system (e.g. Ader et al.,
164 2006) and sealed tube combustion (e.g., Thomazo et al., 2011; Busigny et al., 2013; Ader et

al., 2014). Results obtained at IPGP on bulk and kerogen samples with more than 100 ppm N using sealed tube combustion (and static mass spectrometry) are identical within error to those obtained on the same samples using the classic method (Ader et al., 2006; Ader et al., 2014). In contrast, at IPGP the on-line step heating method was shown to yield non-reproducible and lower N contents and N isotope composition for kerogens and bulk sediments (Ader et al., 2006). Using these static methods, it was demonstrated that for N contents below 100 ppm, it is essential to remove all sources of N-contamination during the sample preparation protocol. This can be achieved by sample degassing under vacuum at temperatures of at least 120°C to remove adsorbed atmospheric N_2 followed by a sample pre-combustion step to remove other types of contamination. This method is preferred for analysis of very low-N rocks (down to 1 ppm) but seems to be less precise, with an error of ± 0.5‰ (2σ) (Busigny et al., 2005; Ader et al., 2006; Thomazo et al., 2011).

The coupling of automatic combustion and purification via an elemental analyzer to an IRMS via continuous flow (hereafter referred to as the CF-EA-IRMS method) is the most widely used technique for $\delta^{15}N$ measurements. However, its application to Precambrian rocks where N contents are usually low has long presented a challenge. The precision of this method is usually ±0.25‰ (1σ) for sediment samples with a N content > 700 ppm (Bahlmann et al., 2010), but reproducibility drops off dramatically at lower N concentrations, requiring additional precautions such as correcting for blanks and ensuring complete sample combustion in order to avoid CO isobaric interferences (Beaumont et al., 1994). Bräuer and Hahne (2005), Papineau et al. (2009), Cremonese et al. (2014) and Stüeken et al. (2015a) described potential pitfalls and sources of error that may arise in analyzing N isotope ratios by CF-EA-IRMS. Yet, because this method is widely accessible and significantly less time-consuming than the traditional method, most recent Precambrian $\delta^{15}N$ data has been acquired

by this method. The quality of results and validation of the technique should nonetheless always be fully discussed.

Two new methods have recently been designed for analyses of samples with very low N content, and these may greatly increase the number of laboratories capable of measuring N isotope ratios in Precambrian rocks: the Nano-EA-IRMS (Polissar et al., 2008), which is an adaptation of the CF-EA-IRMS for smaller samples (but for which blank issues remain), and the combination of sealed-tube combustion with continuous flow IRMS (Bebout et al., 2007; Stüeken et al., 2015b), which dramatically improves blank control. Using the latter method, Stüeken et al. (2015) reproduced the same range of $\delta^{15}N$ values on samples from the ca. 2.7 Ga Tumbiana Formation (Pilbara craton, Australia) as previously obtained by the static method by Thomazo et al. (2011).

It is likely that in the future, *in situ* methods for $\delta^{15}N$ measurement in Precambrian rocks using SIMS types instruments will become increasingly available. These instruments are currently used for $\delta^{15}N$ measurements when variations on the order of several tens of per mil are expected (i.e. extraterrestrial samples and biologic samples of ^{15}N-tracer experiments; Hoppe et al., 2013; Füri and Marty, 2015). To date, their poor reproducibility (>10‰) and lack of adequate N-isotope standards have precluded useful applications to Precambrian samples. Likewise, most *in situ* analyses of N concentrations in Precambrian organic matter have been done by NanoSIMS, but results have been semi-quantitative (Oehler et al., 2010; Wacey et al., 2013; 2014; 2015), or quantitative with poor reproducibility (around 20%; Oehler et al., 2006; 2009; Papineau et al., 2010; Alleon et al., 2015). This is because isotopically homogeneous standards of kerogen and graphitic carbon have seldom been tested and are not widely available. However, we expect this technique to evolve quickly; a recent preliminary report shows that *in-situ* $\delta^{15}N$ measurements on Precambrian microfossils by

NanoSIMS are promising and could yield a precision of ±2‰ (Delarue et al., 2015 Goldschmidt abstract).

The lack of internationally recognized rock and mineral standards for nitrogen isotopes is a major shortcoming in the application of N isotopes to ancient sedimentary rocks. Internal standards are most commonly calibrated against IAEA-N1 and –N2 ammonium sulphate standards and used for the particular applications in each laboratory. Dennen et al. (2006) established two petroleum source rock reference materials (SDO-1, a Devonian Ohio Shale and SGR-1, an Eocene Green River Shale) and a modern marine sediment reference material (PACS-2) as a set of reference materials useful for analysis of ^{13}C, ^{15}N, C and N in organic material in sedimentary rocks. Compared to most Precambrian sedimentary rocks, these rocks have very high TOC and bulk N contents, from 3 to 24% and 0.27 to 0.81%, respectively, and their organic matter is immature so that most their N should belong to kerogen. In Precambrian rocks, organic mater is highly mature and bulk N content is usually very low (from 1 to 1000 ppm), whereas N distribution between kerogen and silicate is highly variable and poorly constrained. Hence, the development of a more suitable suite of rock standards, together with series of organic and inorganic N-isotope standards, would improve the reliability of data measured on ancient rocks.

3. Post-depositional modifications of surface sediment $\delta^{15}N$

In thermally immature sedimentary rocks, N is mostly present as organic-N and fixed-NH_4^+, the latter of which substitutes for K^+ in phyllosilicates (Müller, 1977; Freudenthal et al., 2001). The partitioning between these two species depends mainly on the post-depositional

history of the sediment. In this paper, the term *post-depositional* is used to indicate the sum of the processes affecting sediments following *earliest diagenesis*, defined here as that which occurs in the water column and in the recently deposited sediments that are in diffusional contact with seawater. Post-depositional processes can be subdivided into three main episodes: long-term early diagenesis (driven mostly by microbial activity in sediment isolated from seawater), burial diagenesis (driven mostly by abiotic processes induced by compaction and temperature increase) and metamorphism (including metasomatism; i.e. fluid-rock exchange driven by circulation of external fluids). Our knowledge of the reactions affecting N speciation and its isotopic expression are summarized below for each of these three post-depositional stages.

3.1. Long-term early diagenesis

During long-term early diagenesis, a component of the sedimentary organic matter is microbially remineralized, which liberates N as NH_4^+, N_2, N_2O, NO_2^-, or NO_3^-, depending on O_2 concentration in porewaters. In most platform sediments today, porewaters become anoxic within a few tens of centimeters below the sediment-water interface such that NH_4^+ released by degradation of organic matter below the redoxcline is either oxidized to NO_2^-, NO_3^- or N_2 and/or fixed into clay minerals. Up to 60% of sedimentary N can be bound as NH_4^+ in clays (Kemp and Mudrochova, 1972; Muller, 1977). In spite of a degree of mineralization and variable NH_4^+ fixation in clays, the isotopic composition of the bulk sediment ($\delta^{15}N_{bulk}$) remains fairly constant with depth in most sediments studied to date (Freudenthal et al., 2001; Prokopenko et al., 2006a,b,c; Khozu et al., 2011; Yamaguchi et al., 2010). Hence, in most studied modern sediments, the redistribution of N from the kerogen to the fluid (and possibly to clay minerals) has only small effects on the bulk N isotope budget of the sediments,

indicating that neither organic mineralization nor NH_4^+ fixation in clay minerals significantly fractionates N isotopes.

However, in the case of sediments deposited in the oxygen minimum zones (OMZ's) of the Eastern Subtropical North Pacific region, $\delta^{15}N_{NH4}$ values in the porewaters of the upper 4 m of sediments increase upward from values of +12‰ at depth to +20‰ near the sediment-water interface (Prokopenko et al., 2006a). This pattern is explained by the fact that some microorganisms in the sediment actively transport NO_3^- from the dysoxic to anoxic waters overlying the sediment into the first tens of centimeters of anoxic, NH_4^+-rich sediments (Prokopenko et al., 2013). NO_3^- is then reduced to NO_2^-, which is then consumed during anaerobic anammox reactions that oxidize NH_4^+ to produce N_2 (Kuypers et al., 2005). The anammox reactions strongly enrich the residual NH_4^+ in ^{15}N (Brunner et al., 2013). Although the ^{15}N-enriched NH_4^+ does not seem to have been fixed in clay minerals in proportions high enough to change the bulk sediment $\delta^{15}N$ in this instance, this may not always be the case. In particular, certain intervals of the Proterozoic must have been favorable for such diagenetic ^{15}N enrichment. Until recently most models for the evolution of Proterozoic seawater redox suggested anoxic deepwaters, in which case this process would be unimportant, because no NO_3^- would be available at depth in the water column. However, recent trace metal data suggest that anoxic waters may have covered only 30–70% of the seafloor (Partin et al., 2013; Reinhard et al., 2013). Whereas this estimate still represents an impressive extent of anoxic seafloor surface compared to a few percent today, it nonetheless implies that the remaining seafloor must have been bathed in dysoxic to oxic waters, in which NO_3^- could have been generated and accumulated. Because of the absence of bioturbation, the sediment might nonetheless be anoxic immediately below the sediment-water interface. This configuration would be similar to that of the surface sediments presently intersected by OMZs, surface sediments being anoxic and overlain by nitrate-bearing waters, and would have multiplied the

285 locations where biologically active transport of NO_3^- by bacteria from the water column into
286 surface sediment may have occurred, fuelling anammox and hence possibly increasing
287 $\delta^{15}N_{sed}$. Coupling the $\delta^{15}N$ analyses of the kerogen extract to that of the bulk sample might
288 thus be useful for identifying such environments in the Precambrian. Provided that neither
289 $\delta^{15}N_{NH4}$ nor $\delta^{15}N_{org}$ have been altered by later post-depositional processes, and that $\delta^{15}N_{NH4}$ is
290 not influenced by a contribution from detrital clay minerals, $\delta^{15}N_{ker}$ could be used to infer the
291 nature of N biogeochemical cycling in the water column, while $\delta^{15}N_{bulk} > \delta^{15}N_{ker}$ would
292 suggest NO_3^- bearing dysoxic to anoxic bottom waters.

293

294 *3.2. Burial diagenesis*

295 With increasing burial depth, bacterial activity decreases and thermal maturation (including
296 organic matter oxidation by ferric iron, such as in banded iron formations) becomes the main
297 mechanism by which sedimentary organic matter is altered. Based on a limited number of
298 studies, thermal maturation of organic matter during burial diagenesis does not significantly
299 modify the C/N ratio and N isotopic composition of either bulk sediments or kerogens
300 (Boudou et al., 1984; Macko and Quick, 1985; Rigby and Batts, 1986; Williams et al., 1995;
301 Whiticar, 1996; Rivera et al., 2015). The isotopic composition of NH_4^+ ($\delta^{15}N_{NH4}$), as
302 measured in clay minerals, remains relatively close to both $\delta^{15}N_{org}$ and $\delta^{15}N_{bulk}$ (±2‰;
303 Williams et al., 1995; Mingram et al., 2005). This similarity suggests that NH_4^+ generated
304 from the organic matter is captured by clay minerals in a closed system. If part of the NH_4^+
305 migrates out of the system, then neither migration nor fixation in the mineral phase impart a
306 significant isotope fractionation. It is thus reasonable to assume that burial diagenesis does not
307 modify the bulk rock and kerogen N isotope compositions.

308 *3.3. Metamorphism*

With the onset of very low-grade (anchizonal) metamorphism, the progressive conversion of kerogen to graphite is accompanied by a significant loss of N (referred to as thermal denitrogenation) resulting in a dramatic increase in the C/N of bulk carbonaceous matter (Volkova and Bogdanova, 1989; Daniels and Altaner, 1990, 1993; Boudou et al., 2008). Studies performed on kerogens from coal series showed that $\delta^{15}N_{org}$ does not vary by more than 1‰ from the anthracite (anchimetamorphism) to the semi-graphite stages (lower greenschist facies), in spite of an increase in C/N from ~50 to ~1000 (Ader et al., 1998, 2006; Schimmelmann et al., 2009). This conservative isotopic behavior suggests that the residual organic matter retains its initial $\delta^{15}N_{org}$ value in spite of low grade thermal denitrogenation and that N is released from the organic matter without isotopic fractionation, most probably as NH_4^+ (Ader et al., 2006; Boudou et al., 2008). However, because this conservative isotopic behavior of $\delta^{15}N_{org}$ during low-grade metamorphism has only been documented in studies of coal series characterized by unusually high organic matter content (>50%), which has different proportions of nitrogen functional groups than marine kerogens, it is not clear the pattern holds for typical marine shales.

Denitrogenation is likely not the only process that influences the N content of kerogen during burial metamorphism. Schimmelmann and Lis (2010) observed reaction of NH_4^+ with kerogen during experiments involving hydrous pyrolysis and long-term hydrous heating. Although the isotopic effect associated with these interactions is unknown, it raises the possibility that interaction of kerogen with NH_4^+, derived either internally by denitrogenation or externally from circulating fluids, might alter the nitrogen isotope compositions of the kerogen. Nitrogen enrichments in the aureoles of dike intrusions have been attributed to such processes, but have not shown significant changes in $\delta^{15}N_{org}$ (Schimmelmann et al., 2009; Meyers and Simoneit, 1999). Nonetheless, given the limited scope of previous studies, it

remains possible that hydrous reactions may alter $\delta^{15}N_{org}$ during burial diagenesis and metamorphism.

The fate of NH_4^+ released by thermal denitrogenation of organic matter depends strongly on the rock mineralogy and metamorphic conditions (e.g., Bebout and Fogel 1992; Moine et al., 1994; Busigny et al., 2003; Mingram et al., 2005; Plessen et al., 2010). Together, these factors control the pH and temperature conditions, which in turn determine the NH_4^+/ NH_3 equilibrium (Li et al., 2012). These conditions, along with the presence of specific minerals (probably oxides) and the local oxygen fugacity, also influence the conversion of NH_4^+/NH_3 to N_2 (Moine et al., 1994; Li et al., 2009; Mikhail and Sverjensky, 2014). Hence, NH_4^+ released by organic matter can either escape the system as N_2, NH_3, or even NH_4^+ in migrating fluids, or it can be retained via substitution for K^+ in K-bearing minerals (Juster et al., 1987; Daniels and Altaner, 1990, 1993; Sucha et al., 1994; Mingram et al., 2005). Fixed-NH_4^+ in K-bearing minerals can later be partly devolatilized with increasing metamorphism, generating isotopically lighter N_2 or NH_3, which may migrate out of the rock, decreasing bulk rock N concentrations and increasing $\delta^{15}N_{bulk}$ values (e.g., Svensen et al., 2008; Mingram et al., 2005; Mingram and Brauer, 2001; Bebout and Fogel, 1992; Bebout et al., 1999). The result of devolatilization is that nitrogen isotope compositions will follow a Rayleigh distillation trend with the net isotopic effect increasing with metamorphic grade. Isotopic enrichments of about 1–2‰ have been documented for greenschist facies, with increases of 3–4‰ for amphibolite facies, and up to 6–10‰ for upper amphibolite conditions (Bebout and Fogel, 1992; Bebout et al., 1999; Boyd and Philippot, 1998; Jia, 2006; Mingram et al., 2005; Mingram and Brauer, 2001; Pitcairn et al., 2005; Yui et al., 2009; Plessen et al., 2010; Haendel et al., 1986). Therefore, significantly fractionated $\delta^{15}N_{bulk}$ values in metasedimentary rocks can be produced by the cumulative effects of prograde metamorphism. However, a number of cases have also been reported for which devolatilization is minimal and $\delta^{15}N_{bulk}$

are hardly modified even for metamorphic grades reaching eclogite or granulite facies (Busigny et al., 2003; Palya et al., 2011). Finally, it is also possible for metamorphic rocks to acquire N if exposed to external fluids rich in NH_3 or NH_4^+. This process has been little studied, except in the case of ore mineralization for which it has been shown that fixed-NH_4^+ contents increased due to fluid migration (e.g., Sterne et al., 1982; Jia and Kerrich, 1999, 2000; Glashmacher et al., 2003; Svensen et al., 2008). It seems likely that this process is common in metamorphic rocks, but it has yet to be geochemically and petrographically documented.

3.4. Challenges in identifying post-depositional modifications of $\delta^{15}N_{sed}$ in Precambrian sedimentary rocks

Because Precambrian sedimentary rocks have undergone a complex post-depositional history, including some degree of metamorphic alteration, doubts often remain as to the integrity of both $\delta^{15}N_{NH4}$ preserved in the mineral phase and $\delta^{15}N_{org}$ preserved in kerogen. Consequently, the significance of $\delta^{15}N_{bulk}$ signatures should always be questioned. Several strategies are employed to identify metamorphic and metasomatic effects on $\delta^{15}N_{NH4}$. For example, an inverse correlation between $\delta^{15}N_{bulk}$ and N content is a strong indicator of metamorphic devolatilization (e.g., Svensen et al., 2008; Mingram et al., 2005; Mingram and Brauer, 2001; Bebout and Fogel, 1992). However, the opposite is not necessarily true, such that the absence of an inverse relationship does not verify that devolatilization did not occur. Correlations between $\delta^{15}N_{bulk}$ and trace elements sensitive to fluid-rock exchange (such as large ion lithophile elements) may also indicate N loss (Busigny et al., 2003; Busigny and Bebout, 2013) or gain due to fluid-rock exchange with NH_4^+-bearing external fluids (e.g., Svensen et al., 2008; Jia and Kerrich 2004b; Kerrich et al., 2006). Finally, assuming that $\delta^{15}N_{org}$ and

$\delta^{15}N_{bulk}$ should not evolve identically during post-depositional alteration processes, a close match between these two values implies that they have not been significantly altered. Consequently, in spite of the laborious extractions of kerogen using concentrated HF required to measure $\delta^{15}N_{ker}$, many recent $\delta^{15}N$ studies on Precambrian sedimentary rocks have reported both kerogen and bulk N isotope compositions (Godfrey and Falkovski, 2009; Godfrey et al., 2013; Kump et al., 2011; Stüeken et al., 2015a,b). The results from these studies show moderately higher $\delta^{15}N$ values in bulk rocks compared to kerogens, with offsets generally lower than 4‰, but reaching up to 13‰ in metasomatized rocks (Godfrey et al., 2013) (Fig. 2). Based on present state of knowledge, these offsets cannot be unambiguously ascribed to metamorphic devolatilisation. Several alternate hypotheses outlined below should be tested in the future.

One potential source of offset in kerogen isotopic values is contamination during HF extraction. An example of contamination was identified by mass balance in the case of kerogens extracted from semi-graphites (Ader et al., 2006). The contaminant was not unambiguously identified, but the formation of insoluble NH_4-bearing fluoride precipitates during HF dissolution was a probable cause, with the NH_4^+ originating from the dissolved silicate phase, from dissolution of atmospheric NH_3/NH_4^+ into the HF-solution during the kerogen extraction procedure, or from trapping of atmospheric NH_3/NH_4^+ by fluoride salts during kerogen storage. In the case of low TOC Precambrian rocks, the proportion of fluoride versus kerogen would be very high, maximizing the likelihood that even a small amount of contamination would yield significant isotopic effects. As discussed by Yamaguchi (2002) and Stüeken et al. (2015), contamination of this sort may explain the several per mil variability of some Precambrian $\delta^{15}N_{org}$ values (e.g. Beaumont and Robert, 1999) both within and between kerogen extractions. A protocol for identifying contaminated kerogens from N-poor rocks must therefore be applied (see for example van Zuilen et al., 2005).

$\delta^{15}N_{org}$ may also evolve during post depositional processes. The observation that $\delta^{15}N_{org}$ does not change with increasing metamorphism of coals (Ader et al., 2006) may not translate to Precambrian sedimentary rocks. The nature of organic matter in Precambrian sedimentary is variable, but in general it comprises only a minor component of the rock, and its structure and reactivity is presumably distinct from coals. It may thus evolve differently during thermal maturation, in particular because the mechanisms of thermal denitrogenation and their isotope effects may be strongly influenced by lithology. Finally, kerogen may have reacted with NH_4^+ originating either from its own denitrogenation or from external fluids, modifying its $\delta^{15}N_{org}$ signature. This explanation could account for results obtained by Godfrey et al. (2013) where $\delta^{15}N_{org}$ values from metasomatized Proterozoic rocks are up to 8‰ lighter than values from unmetasomatized rocks from the same basin. Interestingly, in metasomatized rocks, $\delta^{15}N_{bulk}$ is only about 4‰ heavier than in the unmetasomatized samples, which suggests that fixed NH_4 may have been less severely perturbed than kerogen by metasomatism.

Another possible source of offset between bulk and kerogen is inheritance from an early diagenetic increase of porewater $\delta^{15}N_{NH4+}$ in anoxic surface sediments lying below oxygenated waters that experienced anammox (Prokopenko et al., 2006a; 2013). In this case, higher $\delta^{15}N_{bulk}$ than $\delta^{15}N_{ker}$ would imply an early diagenetic environment influenced by nitrate diffusion into anoxic pore waters, provided that neither $\delta^{15}N_{org}$ nor $\delta^{15}N_{NH4}$ are altered by later post-depositional processes. A final potential offset is a contribution to the bulk signature from a detrital silicate phase containing ammoniated minerals (i.e. illite) with a distinct N-isotope signature (e.g. Schubert and Calvert, 2001). In this case, the $\delta^{15}N_{bulk}$-$\delta^{15}N_{ker}$ offset could be either positive or negative.

Given the potential implications of the differences between $\delta^{15}N_{bulk}$ and $\delta^{15}N_{org}$ for reconstructing Precambrian environments, more focused studies on the effects of

metasomatism, metamorphism, initial lithology and type of organic matter on $\delta^{15}N_{bulk,}$ $\delta^{15}N_{NH4+}$ and $\delta^{15}N_{org}$ are required to determine controlling mechanisms on N isotopic distributions in variably altered rocks.

4. Transmission of the $\delta^{15}N$ signal from primary producers to surface sediments: earliest diagenesis isotope effects

Most N in modern sediments originates from sinking particulate organic matter, sometimes with a lesser contribution from detrital clay minerals. Since this particulate organic matter is ultimately derived from primary productivity in the photic zone, $\delta^{15}N_{sed}$ should reflect the initial primary producers provided that isotope modifications accompanying biodegradation in water column and surface sediment can be estimated or are negligible. Two broad patterns of N-isotopic behavior during earliest diagenesis have been identified. The nature of these patterns depends mainly on O_2 exposure time, a parameter that integrates water column oxygenation, the duration of particle sinking (a function of water depth and particle size), and the sealing efficiency (driven by sedimentation rates) that influence the residence time of organic matter at the sediment-water interface.

Sedimentary organic matter that has experienced long O_2 exposure times—i.e. when deposited below a deep water column, under low sedimentation rates, or at high O_2 concentration (all of which characterize modern deep sea sediments)—is commonly enriched in $\delta^{15}N$ by +3 to +5‰ compared to surface particulate organic matter (Robinson et al., 2012; Altabet et al., 1999; Sachs and Repeta, 1999; Brummer et al., 2002; Nakanishi and Minagawa, 2003; Gaye et al., 2009; Möbius et al., 2010; Möbius et al., 2011; Prahl et al., 2003). This

454 ^{15}N-enrichment is consistent with an increase up to 3‰ in sedimentary δ^{15}N observed in a
455 laboratory experiment conducted in oxic conditions (Lehmann et al., 2002) and in reoxidized
456 sapropels and turbidites (Cowie et al., 1998; Prahl et al., 2003; Moodley et al., 2005; Möbius
457 et al., 2010). The causes and detailed mechanisms of this isotopic alteration are still under
458 investigation, but its magnitude was shown to correlate with the extent of amino acid
459 degradation under oxidizing conditions (Gaye et al., 2009; Möbius et al., 2010; Möbius et al.,
460 2011), suggesting that the most labile constituents of primary organic matter are relatively
461 ^{15}N-depleted.

462 Organic matter having experienced minimal O_2 exposure time, i.e. when deposited in shallow
463 marine environments, under high sedimentation rates (e.g. in deltas), and/or in O_2-depleted
464 waters, has similar or slightly lower δ^{15}N values (within <1‰) than surface water particles
465 (Altabet et al., 1999; Pride et al., 1999; Emmer and Thunell, 2000; Lehmann et al., 2002;
466 Kienast et al., 2002; Thunell and Kepple, 2004; Möbius et al., 2010; Chen et al., 2008). This
467 conformity between the δ^{15}N values of primary producers and sedimentary organic matter is
468 confirmed by δ^{15}N analyses of total N and chlorins N (degradation products of chlorophyll) in
469 sediments deposited in stratified waters of the eastern Mediterranean during the Quaternary.
470 These data show that $\delta^{15}N_{sed}$ values reflect the isotopic composition of N used by biomass
471 without significant alteration (Sachs and Repeta, 1999; Higgins et al., 2010). This scenario is
472 compatible with the observation of a slight (< 1‰) decrease in δ^{15}N of suspended particles
473 and/or surface sediment in anoxic water bodies (Libes and Deuser, 1988; Fry et al., 1991;
474 Velinsky et al., 1991; Voss et al., 1997) and with results of laboratory experiments conducted
475 under anoxic conditions (Lehmann et al., 2002). The slight decrease in δ^{15}N is usually
476 interpreted as resulting from the addition of chemoautotrophic bacterial biomass depleted in
477 ^{15}N by NH_4^+ assimilation (Fry et al., 1991; Velinsky et al., 1991; Coban-Yildiz et al., 2006;
478 Chen et al., 2008; Voss et al., 1997), chemoautotrophic fixation of ^{15}N-depleted N_2

(Fuchsman et al., 2008), and/or chemoautotrophic fixation of ^{15}N-depleted N_2O released by denitrification at the transition from suboxic to anoxic waters (Westley et al., 2006).

Most extant Precambrian sedimentary rocks were deposited in platform settings rather than in the deep oceans, most commonly in water columns deficient in O_2 compared to the present-day ocean (e.g. Holland, 2006; Lyons et al., 2014). It is thus generally assumed that early diagenesis has not significantly modified primary $\delta^{15}N$ signature and that $\delta^{15}N_{sed}$ mostly records the isotopic composition of primary producers. However, whereas the modern marine N cycle has complex trophic chains dominated by eukaryotic primary productivity and strongly influenced by the ballasting of particulate organic carbon, Precambrian ecosystems would have been simpler, primary production being dominated by cyanobacteria that produced slowly sinking organic particles (Logan et al., 1995; Lenton et al., 2014; Butterfield, 2015). Given the susceptibility of N isotope signatures to alteration of primary organic matter in the water column and during early diagenesis and the role of ocean redox, the modern ocean is an imperfect analogue for Precambrian ecosystems. In this respect, it will be necessary to develop trophic chain models appropriate for Precambrian microbial ecosystems in order to fully exploit and interpret $\delta^{15}N_{sed}$ in the ancient record.

5. Isotopic fingerprints of primary producers in the modern ocean

The N isotope composition of primary producers at a given time and location depends on the isotope composition of their available N sources (mostly NH_4^+, NO_3^-, dissolved organic nitrogen (DON) and N_2) and on the isotope fractionation associated with N-assimilation pathways: ammonium assimilation, nitrate assimilation and N_2-fixation, respectively (Fig. 3).

We review below the current state of knowledge on how the availability and isotope composition of N-sources in the photic zone is linked to the behavior of the modern N cycle.

Ammonium is released during remineralization of organic matter with minimal isotope fractionation (Prokopenko et al., 2006b,c; Möbius, 2013). In the oxic surface waters of the modern ocean, any NH_4^+ released by breakdown of organic matter is immediately and typically quantitatively nitrified via sequential oxidation to NO_2^- and NO_3^-, in most cases erasing any isotope fractionation associated with nitrification. In rare cases where the oxidation is incomplete, the residual NH_4^+ is enriched in ^{15}N (e.g., Granger et al., 2011), owing to the first oxidation step to nitrite (NO_2^-), which involves a large fractionation ($\varepsilon_{NO2-NH4} \sim -41‰$ to $-13‰$; Casciotti et al., 2003; Mariotti et al., 1981; Santoro and Casciotti, 2011). The isotopic fractionation associated with NH_4^+ assimilation favors the incorporation of ^{14}N and can be large ($\varepsilon_{org\text{-}NH4} \sim$ -10‰ to −27‰, Pennock et al., 1996; Hoch et al., 1992; Vo et al., 2013), but it decreases strongly with NH_4^+ availability, and no fractionation is expressed when it is entirely consumed. Hence, although nitrification and ammonium assimilation may strongly fractionate N isotopes, these fractionations are rarely expressed in modern photic zones where the recycled N is quantitatively re-assimilated into biomass.

Nitrate in the euphotic zone is produced by nitrification of remineralized NH_4^+ and supplied by continental runoff and upwelling. Its assimilation entails fractionation with $\varepsilon_{org-NO3}$ between 0 and −10‰ in NO_3^--limited and NO_3^--replete conditions, respectively (Fogel and Cifuentes 1993; Pennock et al., 1996; Bauersachs et al., 2009). Nitrate is generally a limiting nutrient and hence nearly fully utilized in surface waters such that little to no isotope fractionation is expressed, except in some locations where other nutrients (usually PO_4^{3-} or Fe) limit the primary productivity (Altabet and François, 1994; Altabet, 2001; Schubert and Calvert, 2001; Somes et al., 2010).

The distribution and fate of DON in the modern ocean, in particular its possible assimilation by primary producers, remain poorly constrained (Bronk et al., 2007; Letscher et al., 2013). However, nitrogen isotope composition of DON is usually close to that of the particulate organic matter (e.g. Knapp and Sigmann, 2005), suggesting that the processes governing its fate, including its assimilation by primary producers, do not impart a strong nitrogen isotope fractionation.

Some autotrophs can also fix molecular N_2 into organic matter (N_2-fixation). These diazotrophs are mainly cyanobacteria, and they generally (but not exclusively) fix N_2 when bioavailable N (i.e. NH_4^+ and NO_3^-) is the limiting nutrient in the surface ocean, provided that PO_4^{3-}, Fe and possibly other nutrients are not limiting (Sohm et al., 2011). For instance, in regions of high PO_4^{3-} availability (e.g., upwelling zone), NO_3^- is depleted and primary producers compensate by fixing N_2. The dominant nitrogenase enzyme in the modern ocean uses Mo as a cofactor and accomplishes N_2 assimilation with minimal fractionation ($\varepsilon_{org-N2} \approx -3$ to +1‰; Hoering and Ford, 1960; Delwiche and Steyn, 1970; Minagawa and Wada, 1986; Macko et al., 1987; Carpenter et al., 1997; Zerkle et al., 2008; Bauersachs et al., 2009; Zhang et al., 2014). N_2 fixation using V- and Fe-only nitrogenases can induce greater N isotope fractionation ($\varepsilon_{org-N2} \approx -7$ to -3‰; Zhang et al., 2014), but these are seldom active in the modern environment. Consequently, in the modern surface ocean, N_2 fixation contributes N with an isotopic composition close to that of the atmosphere (0‰) to the bioavailable N pool.

Given these sources of bioavailable N, $\delta^{15}N$ of primary producers reflects the isotope balance of the assimilated N sources: NH_4^+, NO_3^- and possibly DON recycled from organic matter in the euphotic zone, upwelled NO_3^- (and possibly DON), and biological N_2 fixation. Integrated over the long time period typical of sediment accumulation, $\delta^{15}N_{sed}$ will thus reflect mainly the relative proportions and isotope balance of deep-water NO_3^- supplied to the euphotic zone and biological N_2 fixation (e.g., Galbraith et al., 2008; Sigmann et al., 2009; Somes et al.,

552 2010; Altabet et al., 2002). The amount and isotope composition of upwelled NO_3^- is strongly
553 controlled by redox conditions in the water column and sediments. Under dysoxic to anoxic
554 conditions, NO_3^- is converted into gaseous species (N_2O and/or N_2) by an incompletely
555 understood combination of metabolic pathways that includes heterotrophic denitrification and
556 anammox, nitrification, NO_3^- reduction, chemolithotrophic sulfide-dependent denitrification
557 (Lam et al., 2009; Lam and Kuypers, 2011; Lavik et al., 2009; Dalsgaard et al., 2012; De
558 Brabandere et al., 2013), and likely other metabolisms yet to be identified. This loss of
559 bioavailable N occurs in OMZs as well as in water column and sedimentary redox fronts
560 where the anaerobic condition required for anammox and denitrification and the aerobic
561 condition for nitrification are satisfied. In present day OMZs, NO_3^- loss is not quantitative and
562 the isotope fractionation is similar to that determined experimentally for heterotrophic
563 denitrification (ε_{NO3-N2} ~+15 to +30‰; Granger et al., 2008; Mariotti et al., 1981), leading to
564 pronounced ^{15}N-enrichment of the residual nitrate (Cline and Caplan, 1975; Brandes et al.,
565 1998; Voss et al., 2001). In redox fronts the isotope fractionation can be lower (ε_{NO3-N2} ~
566 +10‰; $\varepsilon_{NH4+-N2}$ ~ +11‰; Wenk et al., 2014). When the redox front is located in the
567 sediments, NO_3^- consumption often proceeds to completion so that the isotope enrichment is
568 only weakly expressed (Kessler et al., 2014; Lehmann et al., 2004 and 2007). If most N loss
569 in the ocean occurs in the upper sediment column, the isotopic composition of the residual
570 NO_3^- only marginally increases, whereas if most of it occurs in OMZs, the isotope
571 composition of the residual NO_3^- increases markedly. Redox conditions in the upper sediment
572 column and the water column thus tightly control both the N loss and the isotope composition
573 of the residual NO_3^- pool that is ultimately returned to the surface waters (Brandes and Devol,
574 2002). In turn, loss of bioavailable N indirectly controls N_2-fixation, within the limits imposed
575 by the availability of other nutrients, specifically PO_4^{3-}, Fe, and Mo (Ganeshram et al., 2002;

Karl et al., 2002; Deutch et al., 2007; Glass et al., 2010; Straub et al., 2013; Moore et al., 2013).

Due to the spatial variability in the parameters regulating NO_3^- losses and N_2-fixation—dependent mainly on ocean circulation patterns, redox conditions in deep and intermediate waters and the depth of the redoxcline in sediments—strong regional and lateral variations in the $\delta^{15}N$ of nitrate, primary producers, and hence sinking organic matter are expected. The heterogeneous nature of $\delta^{15}N$ in the modern marine nitrate reservoir and in surface sediments captures this range of variation, with a mode at 5–6‰, a small negative tail approaching 1‰ and a large positive tail to +15‰ corresponding to OMZs (Somes et al., 2010; Tesdal et al., 2013).

One of the key parameters in interpreting N isotope compositions in ancient sediments is the isotope composition of atmospheric N_2. Although this has been a matter of debate in the past (Jia and Kerrich, 2004a; Kerrich et al., 2006), we consider here that it has remained close to 0‰ for at least the past 3.5 Ga, on the basis that $\delta^{15}N$ data obtained on N_2 from fluid inclusions in sedimentary cherts spanning most of Earth history are close to 0‰ (±2 to 3‰, Sano and Pillinger, 1990; Nishizawa et al., 2007; Marty et al., 2013). Consequently, we assume in the following discussion that changes in $\delta^{15}N_{sed}$ can be interpreted in terms of modifications of the ocean N cycle, which controls the abundances of NO_3^-, NO_2^-, and NH_4^+ and their N isotope compositions.

The Precambrian N cycle must have evolved through different stages presumably much different from the present-day N cycle. Two likely causes for differences in the N cycle were the balance of available nutrients (Anbar and knoll 2002; Saito et al., 2003: Glass et al., 2009) and the population of organisms exploiting key N metabolic pathways. Much recent attention has been focused on the timing of evolution of diazotrophic lineages (e.g. Stüeken et al.,

2015a; Sanchez-Barcaldo et al., 2014; Zhang et al., 2014), which should have a very strong impact on the marine N cycle because N_2 fixation is by far the dominant source of new bioavailable N in the modern ocean (e.g., Fennel et al., 2005; Canfield et al., 2010). In the absence of N_2 fixation, not only must other N sources with distinct isotope compositions be considered (e.g. Stüeken et al., 2015a), but also losses of bioavailable N must have been less important quantitatively (e.g. Fennel et al., 2005; Canfield et al., 2010; Thomazo and Papineau, 2013). Along the same lines, based on a marked increase in the range of $\delta^{15}N_{ker}$ values in Precambrian sedimentary cherts at the Great Oxidation Event (GOE), Beaumont and Robert (1999) suggested that the oxidative N cycle became dominant ca. 2.2 Ga. The timing of this divergence has been progressively pushed back with the acquisition of new data and is now 2.7 Ga (e.g., Garvin et al., 2005; Thomazo et al., 2011). However, even if such biogeochemical innovations were unambiguously identified in the sedimentary record, it would remain a formidable challenge to discriminate between an innovation in the behavior of the global N cycle and a local environmental signal.

It is also possible that the isotope fractionations associated with N metabolic pathways have changed over Earth's history. Zhang et al. (2014) recently presented an example of the potential evolution of the N isotope phenotype and its consequences on the interpretation of $\delta^{15}N_{sed}$. In their experimental study, they found that N_2-fixation, when performed by nitrogenase using V or Fe as cofactors, instead of the more common Mo cofactor, entails a significantly different fractionation: $\varepsilon_{org-N2} \approx$ -7 to -3‰ versus $\varepsilon_{org-N2} \approx$ -3 to +1‰, respectively. Because Mo may have been scarce during periods of atmospheric and/or oceanic anoxia, this significantly different isotopic expression for N_2-fixation opens the door to alternative explanations for anomalously low $\delta^{15}N_{sed}$ signatures. For example, the typical $\delta^{15}N_{sed}$ values of -2 to -4‰ in Cretaceous OAE-2 black shales may reflect a shift to V and Fe nitrogenase-dominated diazotrophy due to Mo-limited ocean anoxia (Zhang et al., 2014)

625 rather than widespread NH_4^+ availability and assimilation in the surface ocean (cf. Junium et
626 al., 2007; Higgins et al., 2012).

627 Finally, because the availability and isotope composition of NO_3^-, and NH_4^+ in the euphotic
628 zone depends strongly on the complex network of redox dependent metabolic pathways by
629 which N flows between reservoirs, the mixing and redox structure of the oceans are bound to
630 exert a strong control on both globally integrated and local $\delta^{15}N_{sed}$ signatures. Emerging
631 models of atmospheric and ocean evolution through Earth's history suggest that Precambrian
632 oceans passed through a series of stable redox stages during progressive oxygenation of the
633 atmosphere (e.g. Holland, 2006; Poulton and Canfield, 2011; Lyons et al., 2014). Presumably,
634 N, like C, S, P, Fe, and other biogeochemically important elements, would have cycled
635 differently during each of these stages, with a manifestation in the $\delta^{15}N_{sed}$ record (e.g.
636 Canfield et al., 2010; Anbar and Knoll, 2002; Saito et al., 2003; Glass et al., 2009; Godfrey
637 and Glass, 2011).

638

639 **6. Conceptual scenarios for the redox structure, nitrogen cycle and $\delta^{15}N_{sed}$ distribution**
640 **of Precambrian oceans**

641

642 Having evaluated the extent to which the $\delta^{15}N$ of primary producers reflects the mass and
643 isotope balance of the N sources utilized by phytoplankton, the next step is to question
644 whether the speciation and isotope composition of the N source are likely to be affected by
645 changes in the N-biogeochemical cycle. Many different scenarios for N sources can be
646 envisaged given the combination of the different redox structures proposed for the
647 Precambrian ocean, in particular if unidirectional changes in N cycling due to evolution of the

main lineages operating key metabolic pathways of the N cycle are taken into account. Rather than evaluate all possible scenarios (which is beyond the scope of this review), we have chosen to focus on a few conceptual scenarios for $\delta^{15}N_{sed}$ patterns in non-actualistic Precambrian oceans. These different cases are constructed based on three main assumptions: 1) the major metabolic pathways involving N had evolved even if they were not necessarily operational due to environmental controls on the availability of their N-substrate; 2) the fractionation factors associated with these metabolisms were the same as the ones known today; and 3) the isotope effects associated with short-term early diagenesis (i.e. N transfer from primary producers to the sediment) were also similar to those occurring in the modern ocean.

6.1. Dominantly oxic oceans: analogy with the modern ocean

The present day ocean (Fig. 4a) is our best example to understand controls on the bioavailable sources and isotope compositions of N in a fully oxygenated global ocean. Although this scenario is widely thought to be mostly a Phanerozoic phenomenon, an increasing number of studies propose that at least low dissolved O_2 levels may have existed outside of expanded OMZs and restricted basins since the GOE (e.g. Partin et al., 2013; Reinhard et al., 2013; Ader et al., 2014; Sperling et al., 2014) (Fig. 4b). In this case, anoxia may have been restricted to below the sediment-water interface in a significant portion of the oceans, with an oxycline probably very close to or at the water-sediment interface. One of the key arguments for this idea is that it is very unlikely that physical stratification of the ocean could be maintained for long period of times, such that even at modest pO_2, the oceans should be oxygenated at depth given a reasonably low nutrient availability (Canfield, 1998). Due to

672 the spatial variability in parameters regulating NO_3^- losses and N_2-fixation in such an ocean—
673 dependent mainly on ocean circulation patterns, redox conditions in deep and intermediate
674 waters and the redoxcline depth in the upper sediment—the mode of the $\delta^{15}N_{sed}$ distribution
675 should be representative of the degree of ocean oxygenation (e.g. Quan and Falkowski, 2009).
676 For example, strongly oxygenated oceans should experience limited NO_3^- loss and hence little
677 ^{15}N-enrichment, resulting in a $\delta^{15}N_{sed}$ mode close to 0‰. There is no known example of this
678 scenario in modern oceans, but it has been proposed by Algeo et al. (2014) for the early
679 Paleozoic and Mezozoic. With more prevalent water column deoxygenation but non-
680 quantitative NO_3^- loss in OMZs, the mode in $\delta^{15}N_{sed}$ should increase, as in the present day
681 ocean, which has a modal value of +6‰ (Tesdal et al., 2013; Fig. 5a). When the oxygen
682 concentration in the ocean is sufficiently low for NO_3^- loss to approach completion in sulfidic
683 OMZs, and/or to limit nitrification of organic matter, the $\delta^{15}N_{sed}$ mode should decrease again,
684 reflecting the increasing input of atmospheric N_2 by N_2-fixers (Boyle et al., 2013).

685

686 *6.2. Redox-stratified oceans*

687

688 A redox-stratified ocean with oxic surface waters and anoxic deep waters is the most common
689 scenario envisaged for Proterozoic oceans (e.g. Lyons et al., 2014). An ocean with this
690 structure may have prevailed between ca. 2.4 Ga, which marks the onset of the GOE when the
691 atmosphere and the surface ocean became oxygenated, and the ca. 0.7–0.5 Ga Neoproterozoic
692 oxidation event (NOE), when the deep ocean is suspected to have become oxygenated (see
693 review in Och and Shields-Zhou, 2012; Lyons et al., 2014). A similar redox structure is also
694 suspected to have been common in restricted and semi-restricted basins during the

Phanerozoic as manifested in Ocean Anoxic Events (OAEs) and Mediterranean sapropels (e.g. Meyers, 2006; Jenkyns, 2010; Tribovillard et al., 2013).

Several present-day redox-stratified systems can be used as analogues for establishing a conceptual model of the N-cycle for this redox scenario, such as the well-studied Black Sea, the Cariaco Basin (Venezuela), and Lake Lugano (Italy). These systems present a permanent redox transition zone separating oxic surface waters from anoxic deep waters (Fig. 4c). As in the modern ocean, only part of the primary productivity is supported by the assimilation of NH_4^+ and NO_3^- recycled within the photic zone. Organic matter export to the deep waters and sediments removes N from the photic zone, which needs to be compensated by other N sources in order for the primary productivity to be maintained. Remineralization generates NO_3^- above the redox transition zone and NH_4^+ below. Nitrate is depleted by assimilation in the euphotic zone. It can accumulate at depth, but only down to the redox transition zone. Within the redox transition zone both NO_3^- (diffusing from above) and NH_4^+ (diffusing from below) are quantitatively converted to N_2 or N_2O by coupled nitrification, heterotrophic denitrification and anammox (Fuchsman et al., 2008; Konovalov et al., 2008; Meckler et al., 2007; Thunell et al., 2004; Wenk et al., 2013). The net result of these processes in this environment is extensive loss of bioavailable N (especially NO_3^- and NH_4^+). If bioavailable N recharge of surface waters is limited to diffusion from slightly deeper waters or by occasional storm induced water column mixing (Fig. 4c), severe bioavailable N limitation develops. If other nutrients are in sufficient supply, bioavailable N deficiency is then compensated by N_2-fixation, which drives surface water $\delta^{15}N_{NO3-}$ toward 0‰ (Quan and Falkowski, 2009). This scenario has been invoked to account for $\delta^{15}N_{sed}$ stratigraphic variations in the Black Sea sediments (Junium et al., 2007; Fulton et al., 2012; Quan et al., 2013) and for $\delta^{15}N_{sed}$ values in Mediterranean sapropels and sedimentary rocks deposited during ocean anoxic events (OAEs; Fig. 5c). It has also been invoked to predict that $\delta^{15}N_{sed}$ values close to 0‰ should

720 characterize the Proterozoic ocean (Anbar and Knoll, 2002). However, closed or semi-closed
721 systems (such as the Black Sea) are not ideal analogues for Precambrian redox-stratified
722 oceans in the sense that their stratification is physically maintained preventing water exchange
723 between surface and deep waters, rather than dynamically maintained by low pO_2 or high
724 organic export.

725 In a conceptual case of dynamically maintained redox stratification in a convecting ocean
726 with downwelling and upwelling currents, the situation would be more complex than in
727 physically stratified systems. The depth of the redoxcline would be expected to vary
728 regionally, and NH_4^+ from anoxic deep waters may locally escape quantitative conversion to
729 N_2 or N_2O in the redox transition zone, for example in upwelling zones (Fig. 4d). ^{15}N-
730 enriched NH_4^+ could then reach the photic zone, where it would be concurrently assimilated
731 and converted to NO_3^- (then also assimilated), yielding positive $\delta^{15}N_{sed}$ signatures (Fig. 4d).
732 This process has been proposed to explain positive $\delta^{15}N$ values in the late Paleoproterozoic
733 Animikie (Godfrey et al., 2013) and Aravalli (Papineau et al., 2009) basins.

734 In a more extreme scenario with a shallow redox transition zone (Fig. 4e), NH_4^+-rich anoxic
735 water may even reach the surface in upwelling zones (Kump et al., 2005). The large isotope
736 fractionation associated with NH_4^+ assimilation in NH_4^+-replete conditions could then
737 produce primary biomass depleted in ^{15}N, leading to negative $\delta^{15}N_{sed}$ signatures, as previously
738 proposed for values as low as −4‰ during OAE2 (Junium et al., 2007; Higgins et al., 2012;
739 Ruvacalba Baroni et al., 2015) and as low as -4.7‰ in the Paleoproterozoic Aravalli
740 Supergroup (Papineau et al. 2009).

741 In summary, in upwelling zones of a redox-stratified ocean, highly variable $\delta^{15}N_{sed}$ values
742 may be expected. This scenario would still involve near quantitative bioavailable N-loss in
743 ocean regions where the redoxcline is undisturbed. The resulting NO_3^- limitation would need

744 to be compensated by N_2-fixation, driving $\delta^{15}N_{sed}$ signatures towards 0‰ or below. In this
745 conceptual model, the $\delta^{15}N_{sed}$ distribution should show a mode between -5 and 0‰,
746 depending mainly on the type of nitrogenase involved (cf. Zhang et al., 2014), but with tails
747 towards more negative and more positive values corresponding to upwelling zones. In the
748 Aravalli Supergroup, shallow-water carbonates and stromatolitic phosphorites have low
749 $\delta^{15}N_{sed}$ values, close to 0‰, whereas deeper water black shales have a large range of $\delta^{15}N_{sed}$,
750 between -4.7 and +26.7‰ (Papineau et al., 2009; 2013; 2016). This large range has been
751 interpreted to result from a relatively shallow redoxcline (caused by high primary productivity
752 fueled by phosphate availability) where strong variations in the relative rates of NH_4^+
753 assimilation and N-loss occurred (Papineau et al., 2009). The $\delta^{15}N_{sed}$ record from the
754 Mesoproterozoic Belt Supergroup, with values close to -1‰ in the deeper part of the basin
755 and close to 5‰ along the margins, is also compatible with such a scenario (Stüeken, 2013).

756

757 *6.3. Fully anoxic oceans*

758

759 Essentially fully anoxic oceans (Fig. 4f) may have prevailed before the evolution of oxygenic
760 photosynthesis and endured throughout the Archean due to rapid consumption of locally
761 produced O_2 in the surface ocean, which prevented O_2 accumulation in the environment to
762 levels that would sustain nitrification (see review in Lyons et al., 2014). After the advent of
763 N_2-fixation, bioavailable N would have been mainly sourced to the ocean by N_2-fixation and
764 subsequent NH_4^+ generation by degradation of organic matter. While the known metabolic
765 pathways oxidizing NH_4^+ all require free O_2 either directly or indirectly (even anammox
766 depends on NO_2^- which requires free O_2; see review in Canfield et al., 2010), NH_4^+ was likely
767 stable in the oceans prior to the advent of oxygenic photosynthesis. Together with dissolved

768 organic N, it would have been the dominant species of bioavailable N. If the pH of the ocean
769 was high enough (~9) to stabilize NH_3 in equilibrium with NH_4^+, the former may have
770 degassed to the atmosphere. Provided that the residence time of NH_3 in the atmosphere
771 allowed it to accumulate in significant proportions, this would have enriched residual NH_4^+
772 (and in turn sedimentary N) in ^{15}N due to the large fractionation between aqueous NH_4^+ and
773 NH_3 (Li et al., 2012). Such a high pH is unlikely for the Precambrian oceans (Grotzinger and
774 Kasting, 1993), but this mechanism has been proposed to explain the high $\delta^{15}N_{sed}$ found in
775 2.7–2.6 Ga lacustrine sediments (Stüeken et al., 2015b). In the case of neutral or acidic
776 oceans, N sinks would be limited to assimilation followed by organic matter burial. In most
777 regions, NH_4^+ assimilation was probably complete preventing the expression of its isotope
778 fractionation. It is only in upwelling regions that an excess of upwelled NH_4^+ might
779 theoretically allow the isotope fractionation associated with NH_4^+ assimilation to be expressed
780 both in the biomass of primary producers and in the residual NH_4^+. In this case, primary
781 organic matter could thus be ^{15}N-depleted where NH_4^+ upwelling reached the euphotic zone,
782 and ^{15}N-enriched downstream of the upwelling zone due to Rayleigh fractionation of the
783 residual NH_4^+ pool. In the absence of N sinks other than sedimentation, the mode of the
784 $\delta^{15}N_{sed}$ distribution should be close to that of N_2-fixation, which could range between -7 and
785 0‰, depending of the type of metal cofactor for the nitrogenase enzyme (Zhang et al., 2014).
786 The overall $\delta^{15}N_{sed}$ distribution could have both negative and positive tails corresponding to
787 upwelling zones. However, this scenario where no NH_4^+ oxidation occurs has not been
788 observed in the modern ocean, nor has evidence for it operating in the past been
789 demonstrated. Furthermore, this process may be unrealistic if it shown that NH_4^+ may serve as
790 an electron donor for anoxygenic photosynthesis, in which case NH_4^+ oxidation may occur in
791 the absence of oxidants. Although it was predicted long ago that inorganic N compounds

could serve as electron donors for anoxygenic photosynthesis (Olson, 1970; Broda, 1977), only recently has such a photosynthetic pathway been documented (Griffin et al., 2007).

Organisms capable of using NO_2^- as the electron donor during photosynthesis are now suspected to be widespread in the modern environment (Schott et al., 2010), and it is possible that the same holds true for NH_4^+ (Teske et al., 1994). In this case, the $\delta^{15}N_{sed}$ distribution of fully anoxic oceans before the advent of oxygenic photosynthesis should be similar to the distributions afterwards, when minute concentrations of O_2 in seawater would have resulted in the oxidation of NH_4^+ to NO_2^- and/or N_2O (Lam and Kuyper, 2011; Mandermack et al., 2009). In turn, NO_2^- would be quantitatively removed from the system by reduction with NH_4^+ either as N_2O or as N_2 by anammox bacteria.

Because NH_4^+ oxidation strongly fractionates N isotopes (Mandermack et al., 2009 and references therein), a whole range of ^{15}N enrichments would be produced in NH_4^+ sedimentary organic matter in which some NH_4^+ was assimilated, depending on the extent of NH_4^+ oxidation (Fig. 4f). In this scenario, because of the loss of ^{14}N-enriched nitrogen, it would be predicted that the $\delta^{15}N_{sed}$ distribution should present a more prominent positive tail than when no NH_4^+ oxidation occurs, with a mode possibly slightly higher than 0‰, depending on the relative importance of N-loss processes (Fig. 4f). The closest modern analogue available for this scenario is Lake Kinneret (also referred to as the Sea of Galilee in the Middle East). During overturning events, NH_4^+ accumulated in the anoxic bottom waters of Lake Kinneret is mixed into the oxygenated surface waters where it is completely oxidized and assimilated, producing a transient increase in N isotope compositions of both residual NH_4^+ and surface particulates, with $\delta^{15}N$ values reaching +30‰ and +25‰ respectively (Hadas et al., 2009).

6.4. Utility of the $\delta^{15}N_{sed}$ proxy in identifying modes of N-cycling

The present attempt to predict the shape of the $\delta^{15}N_{sed}$ distribution for several redox scenarios is admittedly simplistic and likely does not capture all the potentially important sources of isotopic variability and complexity. One of the logical next step is to construct spatially resolved ocean circulation models that integrate the redox and the N biogeochemistry together with its N isotope systematics to develop more quantitative predictions of $\delta^{15}N_{sed}$ distributions in different scenarios and at variable spatial scales. This could be started by adding N isotopes to existing models integrating the ocean geometry and mixing dynamics together with the kinetic of metabolic pathways operating the N-cycle, such as those of Al Azhar et al., (2014) and Boyle et al. (2013). Nonetheless, the present qualitative review yields several broad conclusions.

(i) Extrapolating results from a single basin to the global N cycle is difficult due to the intrinsic complexity and heterogeneity of the N cycle. Conversely, $\delta^{15}N_{sed}$ data may be highly useful in reconstructing both temporal and spatial changes of the N-cycle at the regional scale, as demonstrated by many recent studies (Papineau et al., 2009; 2013; 2016; Godfrey et al., 2013; Stüeken, 2013),

(ii) In order to produce a robust assessment of the global N cycle during specific intervals of the Precambrian, $\delta^{15}N_{sed}$ data should be obtained from widely distributed locations and varied depositional environments.

(iii) $\delta^{15}N_{sed}$ distributions alone may be insufficient to discriminate between broadly defined scenarios of N biogeochemical cycling at both basin and global scales. Acquiring independent

environmental and specifically redox constraints (e.g. from trace element abundances) is thus essential for a rigorous interpretation of $\delta^{15}N_{sed}$ distributions in the Precambrian.

7. Secular evolution in Precambrian $\delta^{15}N$ signatures

The Precambrian $\delta^{15}N_{sed}$ database has grown steadily over the last ten years and several papers have recently reported secular variations in $\delta^{15}N_{sed}$ for parts or all of the Precambrian (Papineau et al., 2005; Thomazo et al., 2009, 2011; Thomazo and Papineau, 2013; Ader et al., 2014; Stüeken et al., 2015a,b). Here, we have merged and updated previous compilations into a single database (see supplementary material). In Figure 6, $\delta^{15}N_{bulk}$ and $\delta^{15}N_{ker}$ data are plotted as a function of time. The $\delta^{15}N_{sed}$ temporal resolution displays several gaps, for instance between 3.2 and 3.0 Ga and 2.4 and 2.2 Ga (i.e. during the GOE), and poor coverage between 1.8 and 0.68 Ga. The spatial resolution is also quite poor, most time intervals being represented by data from only one location (supplementary Table). It is thus inevitable that as new data are acquired, some of the features in Figure 6 will change. Due to the importance of the shapes and modes of $\delta^{15}N_{sed}$ distributions in the interpretation of N-isotope data, we also present $\delta^{15}N_{sed}$ distributions for the entire Precambrian (Fig. 5d) and for four time intervals for which data are relatively abundant: 680–540 Ma, 2.2–1.8 Ga, 2.8–2.4 Ga and 3.8–2.8 Ga (Fig. 5e-h). The time intervals 2.4-2.2 Ga and 1.8-0.68 Ga are omitted due to lack of data and poor temporal resolution, respectively.

At this stage, given the heterogeneity of the data set, simple data distributions are presented with no attempt to obtain an equal representation of the studied basins and successions. Certain extensively studied sedimentary successions inevitably dominate some distributions,

as is the case of the Doushantuo Formation in the Yangtze Gorge Area (South China), which strongly dominates the 680–540 Ma interval. Also, no attempt has been made to filter data that may not be representative of normal marine conditions. This might have eliminated many earlier Archean samples, most of them being cherts of possible hydrothermal origin (Pinti and Hashizume, 2001) as well as samples possibly representing Late Archean alkaline lake successions (Stüeken et al., 2015b). As more data are acquired for marine successions from multiple cratons, more meaningful representations of $\delta^{15}N$ variability in the ocean will emerge and the large-scale patterns will surely be revised.

Because the present dataset does not offer sufficient spatial coverage or temporal resolution to obtain meaningful distributions, in principle it would be premature at this stage to try to interpret secular variations of the $\delta^{15}N_{sed}$ distributions in terms of the global marine N-cycle. Nevertheless, we assume in the following discussion that the data is statistically sufficient to identify major features of the Precambrian $\delta^{15}N_{sed}$ record and make preliminary interpretations. The aim of the following discussion is both to illustrate the potential of this proxy for unraveling changes in the N-cycle and to motivate further data collection to refine models for the evolution of the N-biogeochemical cycle through time.

Main features of the Precambrian $\delta^{15}N_{sed}$ record

With the exception of two episodes characterized by highly positive $\delta^{15}N_{sed}$ values (at ca. 2.7 and 1.9 Ga), most Precambrian $\delta^{15}N_{sed}$ data are between -2 and +10‰, with the vast majority clustered more tightly between 0 and +8‰ (Fig. 5d and Fig. 6). This range is intermediate between that of modern ocean surface sediments (Tesdal et al., 2013) and Phanerozoic

884 sediments (Algeo et al., 2014) (Fig. 5a and b). It is worth noting here that for a given time
885 interval, the most positive $\delta^{15}N_{sed}$ values usually are found in bulk samples having
886 experienced metamorphism in excess of greenschist facies, whereas the most negative $\delta^{15}N_{sed}$
887 values are often found in kerogens.

888 The most striking feature observed in Figure 6 is the extremely positive values at ca. 2.7 and
889 1.9 Ga. At 2.7 Ga, these high $\delta^{15}N_{sed}$ values are observed in several basins, with values up to
890 +50‰ in bulk samples and kerogens affected by greenschist facies metamorphism only
891 (supplementary Table, Beaumont and Robert, 1999; Jia and Kerrich, 2004b; Kerrich et al.,
892 2006; Thomazo et al., 2011; Stüeken et al., 2015b). At ca. 1.9 Ga, $\delta^{15}N_{sed}$ values are typically
893 between +10 and +20‰, also reach as high as +27‰. To date, such positive values have been
894 observed in only a few localities associated with unusual stromatolitic phosphorite in the
895 Aravalli Supergroup, northwestern India, and the most positive values are found in bulk
896 samples having experienced metamorphic conditions higher than greenschist facies (Papineau
897 et al., 2009).

898 Subtle evolution with time of the mode of $\delta^{15}N_{sed}$ distribution is also evident (Fig. 5e to h).
899 The 3.8–2.8 Ga interval has the lowest mode (≈ +2‰), with a tight distribution specifically
900 after 3.3 Ga (between -4 and +5‰). The 2.8-2.4 Ga interval has a slightly higher mode (≈
901 +3‰) and the 2.2–1.8 Ga interval an even higher $\delta^{15}N_{sed}$ mode (≈ +5‰). The 680–540 Ma
902 interval presents a mode of ~ +3‰ and a relatively tight $\delta^{15}N_{sed}$ distribution (between -2 and
903 +10‰). Overall, these modes fall between that of the modern ocean and OAE $\delta^{15}N_{sed}$
904 distributions.

905

906 *Effects of post-depositional processes on patterns of $\delta^{15}N$ variations with time*

907

908 As discussed in section 3, detailed petrological and geochemical characterization is still
909 lacking for many samples, such that potential metamorphic effects on $\delta^{15}N_{sed}$ and $\delta^{15}N_{ker}$
910 remain uncertain, even in samples having undergone only greenschist facies metamorphism.

911 Although it is unlikely that the extreme ^{15}N-enriched signatures at 2.7 Ga can be explained by
912 metamorphism (they are identified in several basins and recorded in both kerogen and bulk
913 analyses of samples; Stüeken et al., 2015b), the $\delta^{15}N_{sed}$ distributions presented here, and in
914 particular their mode, may still have been affected to some extent by metamorphism. At least
915 two observations lend support to this possibility: samples having been metamorphosed
916 beyond greenschist facies tend to show comparably high $\delta^{15}N_{sed}$ for a given time interval (Fig.
917 6), and $\delta^{15}N_{sed}$ distributions have a $\delta^{15}N_{bulk}$ mode higher than that of their
918 corresponding $\delta^{15}N_{ker}$ and $\delta^{15}N_{ker}$ distributions (Fig. 5). It is thus critical to better characterize
919 metamorphic grades of analyzed samples in order to better evaluate the potential impact of
920 metamorphism on $\delta^{15}N_{sed}$ values.

921 Another important feature in Figure 6 is that the most negative $\delta^{15}N$ values for a given age are
922 mostly recorded by kerogen, consistent with the observation that $\delta^{15}N_{ker}$ is typically equal to
923 or lower than $\delta^{15}N_{bulk}$ when both are measured on the same sample (Fig. 2). As discussed in
924 section 3.4, this difference may reflect metamorphic effects on $\delta^{15}N_{bulk}$ and/or $\delta^{15}N_{ker}$, but it
925 could also have been acquired at the time of deposition due to a contribution of NH_4-bearing
926 detrital clay minerals or to early diagenetic processes in the water column and surface
927 sediments. Contributions from detrital clay minerals were likely minimal to nil in the
928 Precambrian when terrestrial biomass was small or nonexistent, severely limiting available
929 nitrogen during the pedogenesis. As for early diagenesis, it is unclear which of $\delta^{15}N_{bulk}$
930 and $\delta^{15}N_{ker}$ should be used as the best proxy for the N-biogeochemical cycle because paired

931 $\delta^{15}N_{bulk}$, $\delta^{15}N_{ker}$ and/or $\delta^{15}N_{NH4+}$ have only seldom been investigated in modern sediments
932 (e.g. Peters et al., 1978; Prokopenko et al. 2006a,b,c) or ancient sedimentary rocks
933 (Yamaguchi, 2002; Williams et al., 2005; Higgins et al., 2012; Bauersachs et al., 2009).
934 Solving this issue is thus of utmost importance. A promising approach that has been
935 investigated for more than 15 years is the use of the N isotope composition of chlorin
936 ($\delta^{15}N_{chlorin}$), a biomarker for primary producers (e.g., Sachs et al., 1999; Beaumont et al.,
937 2000; Higgins et al., 2011). However uncertainties remain about the potential offset between
938 $\delta^{15}N_{chlorin}$ and primary producers of past ecosystems (Tyler et al., 2010; Junium et al., 2014)
939 and it is doubtful that it will be possible to extract chlorin from Precambrian samples.
940 Nonetheless, a comparison between $\delta^{15}N_{chlorin}$, $\delta^{15}N_{bulk}$ and/or $\delta^{15}N_{ker}$ in various modern
941 environments may help to better understand how and when water column and surface
942 sediments early-diagenetic processes modify $\delta^{15}N_{bulk}$ and/or $\delta^{15}N_{ker}$ (Sachs and Repeta, 1999;
943 Higgins et al., 2010; Junium et al., 2015). Another promising avenue is to link Raman spectral
944 signature of organic matter to metamorphic grades (Beyssac et al., 2002) as well as X-ray
945 spectroscopy techniques, which can be used to characterize the crystallinity and nitrogen
946 functional groups of organic matter (Papineau et al., 2016). Such analyses of organic matter
947 can be done *in situ* and quantitatively calibrated against other methods like NanoSIMS
948 (Alleon et al., 2015), which will eventually allow for precise *in situ* $\delta^{15}N$ analyses.

949

950 *Effects of changes in the N-biogeochemical cycle on $\delta^{15}N$ distributions with time*

951

952 Assuming the $\delta^{15}N$ signature was not significantly affected by post-depositional processes
953 and can be used to trace changes in the N-biogeochemical cycle, two types of effects could be

954 responsible for modifications in the $\delta^{15}N_{sed}$ distributions: (i) biological innovations, whereby
955 new metabolic pathways become operational and (ii) changes of the ocean redox structure,
956 which controls the activity of metabolic pathways allowing them to become ecologically
957 dominant. The $\delta^{15}N_{sed}$ distribution predicted for the conceptual redox scenarios envisaged in
958 the section 6 showed that although differences might be expected in the mode and in
959 amplitudes of positive and negative tails, these differences should be subtle. This prediction is
960 corroborated by the large amplitude of $\delta^{15}N$ variation for each time interval (Fig. 5 and 6)
961 relative to the small variations in the $\delta^{15}N$ mode with time (Fig. 6). Hence changes in the N
962 cycle, if any, are recorded in small modifications of the distribution mode and shape.

963 Assuming that the variation in $\delta^{15}N_{sed}$ distribution between time intervals is representative,
964 then the lowest mode (+1‰) is found for the 3.5–2.8 Ga time interval when the oceans were
965 probably fully anoxic with minimal N-loss via fractionating oxidative pathways (Fig. 4f). The
966 $\delta^{15}N_{sed}$ signature would thus reflect mostly N_2-fixation (Beaumont and Robert, 1999; Stüeken
967 et al., 2015a). The mode increases to +3‰ in the 2.8–2.4 Ga time interval is consistent with
968 the idea that oxygenic photosynthesis had started to produce O_2, allowing N-loss reactions to
969 proceed (even if O_2 was not significantly accumulating in the environment) (Busigny et al.,
970 2013; Garvin et al., 2009; Godfrey et al., 2009) (Fig. 4f). The extremely positive $\delta^{15}N_{sed}$
971 values at ca. 2.7 Ga could correspond to the transition between these two stages and represent
972 the oxidative distillation of the NH_4^+ reservoir (Thomazo et al., 2011). Unfortunately, a gap of
973 data in the 2.4–2.2 Ga time interval precludes identification of possible changes in N cycling
974 associated with the GOE. Another increase in the $\delta^{15}N$ mode to +5‰ in the 2.2–1.8 Ga
975 interval may reflect the oxygenation of the atmosphere, surface waters and most probably a
976 significant part of deep waters (e.g., Partin et al., 2013; Reinhard et al., 2013), leading to an
977 increase in the surface of redox transitions zones where N-losses occur (Fig. 4b, d or e). In

this scenario the highly positive $\delta^{15}N_{sed}$ recorded in one location at ca. 1.9 Ga would correspond to localized distillation of the NH_4^+ reservoir either by oxidation or assimilation in places where the chemocline impinged on the euphotic zone (Papineau et al., 2009). Although the period following 1.8 Ga is too poorly documented to present a statistically relevant $\delta^{15}N_{sed}$ distribution, the available data do not show any identifiable change in the range of $\delta^{15}N_{sed}$ between the 2.2–1.8 Ga interval and the 0.68-0.54 Ga interval (Fig. 6).

The $\delta^{15}N_{sed}$ record is thus at least broadly consistent with and reflective of the redox evolution widely envisaged for the Precambrian oceans (e.g. Lyons et al., 2014). However, $\delta^{15}N_{sed}$ variations may also be compatible with other redox or paleo-environmental scenarios. For example, the positive $\delta^{15}N_{sed}$ excursions at 2.7 Ga has alternatively been interpreted as a record of N isotope fractionation induced by NH_3 degassing from alkaline lakes (Stüeken et al., 2015b). As another example, the data that dominate the 3.5–2.8 Ga time interval are dominated by cherts, which may be hydrothermal in origin and not representative of normal marine conditions (Pinti and Hashizume, 2001). Hence, although the available $\delta^{15}N_{sed}$ data are tantalizing and appear consistent with models for Precambrian oxygenation, more work is required before we can confidently apply them to reconstructing ancient changes in the marine N-biogeochemical cycle.

8. Conclusions and Perspectives

Although making reliable measurements of $\delta^{15}N_{sed}$ in rocks with low N content remains difficult, a series of recent analytical developments have made these analyses more accessible. Consequently, population of the $\delta^{15}N_{sed}$ database for the Precambrian has accelerated over the

last 10 years. This trend should begin to fill in the $\delta^{15}N_{sed}$ record, which is sparse for several notable time periods, and in particular the 2.4–2.2 Ga interval, which corresponds largely to the GOE, and the 1.8–0.68 Ga interval, roughly corresponding to the so-called "boring billion." In addition, given that the N biogeochemical cycle at the scale of the entire ocean can only be realistically captured by investigating a range of depositional environments from multiple basins, the present dataset is still too limited to be confidently extrapolated to the global ocean even in intervals with abundant data. $\delta^{15}N_{sed}$ data are often available only from a single or limited number of basins for each time interval, such that $\delta^{15}N_{sed}$ distributions do not yet provide a statistically robust record of the spatial $\delta^{15}N_{sed}$ variations in the ocean. In order to capture a synoptic view of the global N-cycle with time, data from multiple coeval sedimentary sequences are necessary, and the available data set should be carefully screened for samples not representative of the marine environment.

The potential modifications of both $\delta^{15}N_{ker}$ and $\delta^{15}N_{bulk}$ during post-depositional processes, as well as their often significant and unexplained differences, are persistent concerns and understanding their origin is essential. Reducing these concerns requires more studies with paired $\delta^{15}N_{ker}$ and $\delta^{15}N_{bulk}$ and/or $\delta^{15}N_{chlorin}$ data for comparison and evaluation of post-depositional modification of nitrogen isotope signatures. Studied sites should be chosen both in well characterized and varied modern environments and in ancient sedimentary settings for which detailed characterization of depositional environments (in particular their redox chemistry) and post-depositional modifications are available.

Because of the complexity of the parameters controlling $\delta^{15}N_{sed}$ spatial variability, numerical modeling may help predict $\delta^{15}N_{sed}$ distributions more reliably for various ocean redox structures and/or evolutionary scenarios (e.g. Ruvalcaba Baroni et al., 2015). This advance will require the addition of N isotopes to models integrating the ocean dynamics with the

kinetics of metabolic pathways regulating the N-cycle, such as has been attempted by Boyle et al. (2013) and Al Azhar et al. (2014). These new models will have to be verified in modern lakes or restricted basins that may serve as analogues for Precambrian oceans.

In spite of these remaining uncertainties, the $\delta^{15}N_{sed}$ frequency histograms established here are compatible with current hypothesis for the Precambrian evolution of ocean redox. Much work remains to develop the $\delta^{15}N_{sed}$ proxy and refine its application to the ancient biogeochemical cycle of N, but the proxy nevertheless shows great promise and is certain to enjoy increasing use in studies of past environments.

Acknowledgments

The transcription of the ideas exposed into the present article benefited greatly from the research dynamics induced by both the Labex UnivEarths program of Sorbonne Paris Cité (ANR-10-LABX-0023 and ANR-11-IDEX-0005-02) and the ANR DZIANI (ANR-13-BS06-0001). This is IPGP contribution 3708.

References

Ader, M., Boudou, J.-P., Javoy, M., Goffe, B., Daniels, E., 1998. Isotope study on organic nitrogen of Westphalian anthracites from the Western Middle field of Pennsylvania (U.S.A.) and from the Bramsche Massif (Germany). Organic Geochemistry 29, 315-323.

Ader, M., Cartigny, P., Boudou, J.-P., Oh, J.-H., Petit, E., Javoy, M., 2006. Nitrogen isotopic evolution of carbonaceous matter during metamorphism: methodology and preliminary results. Chemical Geology 232, 152-169.

Ader, M. Sansjofre, P., Halverson, G.P., Busigny, V., Trindade, R.I.F., Kunzmann, M.,

1048 Nogueira, A.C.R., 2014. Ocean redox structure across the Late Neoproterozoic oxygenation
1049 event: A nitrogen isotope perspective. Earth and Planetary Science Letters 396, 1-13.

1050 Al Azhar, M., Canfield, D.E., Fennel, K., Thamdrup, B., Bjerrum, C.J., 2014. A model-
1051 based insight into the coupling of nitrogen and sulfur cycles in a coastal upwelling system.
1052 Journal of Geophysical Research: Biogeoscience 119, 1–17, doi:10.1002/2012JG002271.

1053 Algeo, T.J., Meyers, P.A., Robinson, R.S., Rowe, H., Jiang, G.Q., 2014. Icehouse-
1054 greenhouse variations in marine denitrification. Biogeosciences, 11: 1273-1295.

1055 Alleon, J., Bernard, S., Remusat, L., Robert, F., 2015. Estimation of nitrogen-to-carbon
1056 ratios of organic and carbon materials at the submicrometer scale. Carbon 84, 290-298.

1057 Altabet, M.A., Francois, R., 1994. Sedimentary nitrogen isotopic ratio as a recorder for
1058 surface ocean nitrate utilization. Global Biogeochemical Cycles 8, 103–116.

1059 Altabet, M.A., Pilskaln, C., Thunell, R., Pride, C., Sigman, D., Chavez, F., Francois, R.,
1060 1999. The nitrogen isotope biogeochemistry of sinking particles from the margin of the
1061 Eastern Tropical Pacific, Deep-Sea Research I 46, 655– 679.

1062 Altabet, M.A., 2001. Nitrogen isotopic evidence for micronutrient control of fractional
1063 NO_3^- utilization in the equatorial Pacific. Limnology and Oceanography 46, 2001, 368–380.

1064 Altabet, M.A., Higginson, M.J., Murray, D.W., 2002. The effect of millennial-scale
1065 changes in Arabian Sea denitrification on atmospheric CO_2. Nature 415, 159–162.

1066 Anbar, A.D., Knoll, A.H., 2002. Proterozoic ocean chemistry and evolution: a
1067 bioinorganic bridge? Science 297, 1137–1142.

1068 Bahlmann, E., Bernasconi, S.M., Bouillon, S., Houtekamer, M., Korntheuer, M.,
1069 Langenberg, F., Mayr, C., Metzke, M., Middelburg, J.J., Nagel, B., Struck, U., Voss, M.,
1070 Emeis, K.C., 2010. Performance evaluation of nitrogen isotope ratio determination in marine

and lacustrine sediments: an inter-laboratory comparison. Organic Geochemistry 41, 3–12.

Bauersachs T, Scouten, S., Compaore, J., Wollenzien, U.I.A., Stal, L.J., Sinninghe Damsté, J.S., 2009. Nitrogen isotopic fractionation associated with growth on dinitrogen gas and nitrate by cyanobacteria. Limnology and Oceanography 54, 1403–1411.

Bauersachs, T., Kremer, B., Schouten, S., Sinninghe Damsté, J.S., 2009. A biomarker and $\delta^{15}N$ study of thermally altered Silurian cyanobacterial mats. Organic Geochemistry 40, 149–157.

Beaumont, V., Agrinier, P., Javoy, M., Robert, F., 1994. Determination of the CO contribution to the $^{15}N/^{14}N$ ratio measured by mass spectrometry. Analytical Chemistry 66, 2187-2189.

Beaumont, V., Robert, F., 1999. Nitrogen isotope ratios of kerogens in Precambrian cherts: a record of the evolution of atmosphere chemistry? Precambrian Research 96, 63–82.

Beaumont, V. I., Jahnke, L.L., Des Marais; D.J., 2000. Nitrogen isotopic fractionation in the synthesis of photosynthetic pigments in Rhodobacter capsulatus and Anabaena cylindrica, Organic Geochemistry 31, 1075–1085.

Bebout, G.E., Cooper, D.C., Bradley, A.D., Sadofsky, S.J., 1999. Nitrogen-isotope record of fluid-rock interactions in the Skiddaw Aureole and granite, English Lake District. American Mineralogist 84, 1495-1505.

Bebout, G.E., Idleman, B.D., Li, L., Hilkert, A., 2007. Isotope-ratio-monitoring gas chromatography methods for high-precision isotopic analysis of nanomole quantities of silicate nitrogen. Chemical Geology 240, 1-10.

Bebout, G.E., Fogel, M.L., 1992. Nitrogen-isotopic composition of metasedimentary rocks in the Catalina Schist, California: implications for metamorphic devolatilization history. Geochimica et Cosmochimica Acta 56, 2839-2849.

1095 Beyssac, O., Goffe, B., Chopin, C., Rouzauf, J.N., 2002. Raman spectra of carbonaceous
1096 material in metasediments: a new geothermometer. Journal of metamorphic geology 20, 859-
1097 871.

1098 Boudou, J.-P., Mariotti, A., Oudin, J.L., 1984. Unexpected enrichment of nitrogen during
1099 the diagenetic evolution of sedimentary organic matter. Fuel 63, 1508-1510.

1100 Boudou, J.-P., Schimmelmann, A., Ader, M., Mastalerz, M., Sebilo, M., Gengembre, L.,
1101 2008. Organic nitrogen chemistry during low-grade metamorphism. Geochimica et
1102 Cosmochimica Acta 72, 1199-1221.

1103 Boyd, S., Hall, A, Pillinger, C.T., 1993. The measurement of $\delta^{15}N$ in crustal rocks by
1104 static vacuum mass spectrometry: Application to the origin of the ammonium in the
1105 Cornubian batholith, southwest England. Geochimica et Cosmochimica Acta 57, 1339-1347.

1106 Boyd, S.R., Phillippot, P., 1998. Precambrian ammonium biogeochemistry: a study of the
1107 Moine metasediments, Scotland. Chemical Geology 144, 257-268.

1108 Boyle, R.A., Clark, J.R., Poulton, S.W., Shields-Zhou, G., Canfield, D.E., Lenton, T.M.,
1109 2013. Nitrogen cycle feedbacks as a control on euxinia in the mid-Proterozoic ocean. Nature
1110 Communication 4, 1533.

1111 Brandes, J.A., Devol, A.H., Yoshinari, T., Jayakumar, D.A., Naqvi, S.W.A., 1998.
1112 Isotopic composition of nitrate in the Central Arabian Sea and Eastern Tropical North Pacific:
1113 A tracer for mixing and nitrogen cycles. Limnology and Oceanography 43,1680–1689.

1114 Brandes, J.A., Devol, A.H., 2002. A global marine-fixed nitrogen isotopic budget:
1115 Implications for Holocene nitrogen cycling. Global Biogeochemical Cycles 16, 1-14.

1116 Bräuer, K., Hahne, K., 2005. Methodological aspects of the ^{15}N analysis of Precambrian
1117 and Palaeozoic sediments rich in organic matter. Chemical Geology 218, 361–368.

1118 Broda, E., 1977. Two kinds of lithotrophs missing in nature. Zeitschrift für allgemeine
1119 Mikrobiologie 17, 491-493.

1120 Bronk, D.A., See, J.H., Bradley, P., Killberg, L., 2007. DON as a source of bioavailable
1121 nitrogen for phytoplankton. Biogeosciences 4, 283–296.

1122 Brummer, G.J.A., Kloosterhuis, H.T., Helder, W., 2002. Monsoon-driven export fluxes
1123 and early diagenesis of particulate nitrogen and its $\delta^{15}N$ across the Somalia margin.
1124 Geological Society, London, Special Publications 195, 353-370.

1125 Brunner, B., Contreras, S., Lehmann, M.F., Matantseva, O., Rollog, M., Kalvelage, T.,
1126 Klockgether, G., Lavik, G., Jetten, M.S.M., Kartal, B., Kuypers, M.M., 2013. Nitrogen
1127 isotope effects induced by anammox bacteria. Proceedings of the National Academy of
1128 Sciences of the USA 110, 18994–18999.

1129 Buick, R., 2007. Did the Proterozoic 'Canfield Ocean' cause a laughing gas greenhouse?
1130 Geobiology 5, 97–100.

1131 Busigny, V., Ader, M., Cartigny, P., 2005. Quantification and isotopic analysis of
1132 nitrogen in rocks at the ppm level using sealed tube combustion technique: a prelude to the
1133 study of altered oceanic crust. Chemical Geology 223, 249-258.

1134 Busigny, V., Cartigny, P., Philippot, P., Ader, M., Javoy, M., 2003. Massive recycling of
1135 nitrogen and other fluid-mobile elements (K, Rb, Cs, H) in a cold slab environment: evidence
1136 from HP to UHP oceanic metasediments of the Schistes Lustrés nappe (western Alps,
1137 Europe). Earth and Planetary Science Letters 215, 27-42.

1138 Busigny, V., Lebeau, O., Ader, M., Krapez, B., Bekker, A., 2013. Nitrogen cycle in the
1139 Late Archean ferruginous ocean. Chemical Geology 362, 115-130.

1140 Busigny, V., Bebout, G.E., 2013. Nitrogen in the Silicate Earth: Speciation and Isotopic
1141 Behavior during Mineral–Fluid Interactions. Elements 9, 353–358.

1142 Butterfield, N.J., 2015. Early evolution of the Eukaryota. Palaeontology 58, 5–17.

1143 Canfield, D.E., 1998. A new model for Proterozoic ocean chemistry. Nature 396, 450-
1144 453.

1145 Canfield, D.E., Glazer, A.N., Falkowski, P.G., 2010. The evolution and future of Earth's
1146 nitrogen cycle. Science 330, 192-196.

1147 Carpenter, E.J., Harvey, H.R., Fry, B., Capone, D.G., 1997. Biogeochemical tracers of
1148 the marine cyanobacterium Trichodesmium, Deep Sea Research Part I 44, 27–38.

1149 Casciotti, K.L., Sigman, D.M., Ward, B.B., 2003. Linking Diversity and Stable Isotope
1150 Fractionation in Ammonia-Oxidizing Bacteria. Geomicrobiology Journal 20, 335-353.

1151 Casciotti, K.L., 2009. Inverse kinetic isotope fractionation during bacterial nitrite
1152 oxidation. Geochimica et Cosmochimica Acta 73, 2061–2076.

1153 Chen, F., Zhang, L., Yang, Y., Zhang, D., 2008. Chemical and isotopic alteration of
1154 organic matter during early diagenesis: Evidence from the coastal area off-shore the Pearl
1155 River estuary, south China. Journal of Marine Systems 74, 372–380.

1156 Cline, J.D., Kaplan, I.R., 1975. Isotopic fractionation of dissolved nitrate during
1157 denitrification in the eastern tropical North Pacific, Marine Chemistry 3, 271–299.

1158 Coban-Yildiz, Y., Altabet, M.A., Yilmaz, A., Tugrul, S., 2006. Carbon and nitrogen
1159 isotopic ratios of suspended particulate organic matter (SPOM) in the Black Sea water
1160 column. Deep-Sea Research Part II, Topical Studies in Oceanography 53, 1875–1892.

1161 Cowie, G., Calvert, S., De Lange, G., Keil, R., Hedges, J., 1998. Extents and implications
1162 of organic matter alteration at oxidation fronts in turbidites from the Madeira Abyssal Plain.
1163 In Proc. ODP, Sci. Results (eds. Weaver PPE, Schmincke H-U, Firth JV, Duffield W) College
1164 Station, TX (Ocean Drilling Program), pp.581-589.

1165 Cremonese, L., Shields-Zhou, G., Struck, U., Ling, H.-F., Och, L., Chen, X., Li, D.,
1166 2013. Marine biogeochemical cycling during the early Cambrian constrained by a nitrogen
1167 and organic carbon isotope study of the Xiaotan section, South China. Precambrian Research
1168 225, 148–165.

1169 Cremonese, L., Shields-Zhou, G., Struck, U., Ling, H.-F., Och, L., 2014. Nitrogen and
1170 organic carbon isotope stratigraphy of the Yangtze Platform during the Ediacaran–Cambrian
1171 transition in South China. Palaeogeography, Palaeoclimatology, Palaeoecology 398, 165–186.

1172 Dalsgaard, T., Thamdrup, B., Farias, L., Revsbech, N.P., 2012. Anammox and
1173 denitrification in the oxygen minimum zone of the eastern South Pacific, Limnology and
1174 Oceanography 57, 1331–1346, doi:10.4319/lo.2012.57.5.1331.

1175 Daniels, E.J., Altaner, S.P., 1990. Clay mineral authigenesis in coal and shale from the
1176 Anthracite region, Pennsylvania. American Mineralogist 75, 825-839.

1177 Daniels, E.J., Altaner, S.P., 1993. Inorganic nitrogen in anthracite from eastern
1178 Pennsylvania, U.S.A. International Journal of Coal Geology 22, 21-35.

1179 De Brabandere, L., Canfield, D.E., Dalsgaard, T., Friederich, G.E., Revsbech, N.P.,
1180 Ulloa, O., Thamdrup, B., 2013. Vertical partitioning of nitrogen-loss processes across the
1181 oxic-anoxic interface of an oceanic oxygen minimum zone, Environmental Microbiology,
1182 doi:10.1111/1462-2920.12255.

1183 Delarue, F., Robert, F., Sugitani, K., Derenne, S., 2015. Archean Microfossils from the
1184 Farrel Quartzite (Pilbara Craton, Australia, 3.0 Gyr) Reveal Contrasted $\delta^{15}N$ Signatures. 25th
1185 Goldchmidt Conference, Prague.

1186 Delwiche, C.C., Steyn, P.L., 1970. Nitrogen isotope fractionation in soils and microbial
1187 reactions, Environment Science and Technology 4, 929– 935.

1188 Dennen, K.O., Johnson, C.A., Otter, M.L., Silva, S.R., Wandless, G.A., 2006. $\delta^{15}N$ and

Non-Carbonate $\delta^{13}C$ Values for Two Petroleum Source Rock Reference Materials and a Marine Sediment Reference Material. USGS, Open-File Report 2006-1071.

Deutsch, C., Sarmiento, J.M., Sigman, D.M., Gruber, N., Dunne, J.P., 2007. Spatial coupling of nitrogen inputs and losses in the ocean, Nature 445, 163– 167.

Falkowski, P.G., 1997. Evolution of the nitrogen cycle and its influence on the biological sequencestration of CO_2 in the ocean. Nature 387, 272-275.

Emmer, E., Thunell, R., 2000. Nitrogen isotope variations in Santa Barbara Basin sediments: Implications for denitrification in the eastern tropical North Pacific during the last 50,000 years. Paleoceanography 15, 377– 387.

Fennel, K., Follows, M., Falkowski, P.G., 2005. The co-evolution of the nitrogen, carbon and oxygen cycles in the Proterozoic ocean. American Journal of Science 305, 526-545.

Fogel, M.L., Cifuentes, L.A., 1993. Isotope fractionation during primary production. In: Engel, M.H., Macko, S.A. (Eds.), Organic Geochemistry, Principles and Applications, pp. 73–98.

Freudenthal, T., Wagner, T., Wenzhöfer, F., Zabel, M., Wefer, G., 2001. Early diagenesis of organic matter from sediments of the eastern subtropical Atlantic: evidence from stable nitrogen and carbon isotopes. Geochimica et Cosmochimica Acta 65, 1795-1808.

Füri, E., Marty, B. 2015. Nitrogen isotope variations in the Solar System. Nature Geoscience 8, 515–522.

Fry, B., Jannasch, H.W., Molyneaux, S.J., Wirsen, C.O., Muramoto, J.A., King, S., 1991. Stable isotope studies of the carbon, nitrogen and sulfur cycles in the Black-Sea and the Cariaco Trench. Deep-Sea Research 38, S1003–S1019.

Fuchsman, C., Murray, J.W., Konovalov, S.K., 2008. Concentration and natural stable

1212 isotope profiles of nitrogen species in the Black Sea. Marine Chemistry 111, 88–103.

1213 Fulton, J.M., Arthur, M.A., Freeman, K.H., 2012. Black Sea nitrogen cycling and the
1214 preservation of phytoplankton $\delta^{15}N$ signals during the Holocene. Global Biocgeochemical
1215 Cycles 26, GB2030, doi:10.1029/2011GB004196.

1216 Galbraith, E.D., Sigman, D.M., Robinson, R.S., Pedersen, T.F., 2008. Nitrogen in past
1217 marine environments. In: Capone, D.G., Bronk, D.A., Mulholland, M.R., Carpenter, E.J.
1218 (Eds.), Nitrogen in the Marine Environment. Elsevier, Amsterdam, pp. 1497-1535.

1219 Ganeshram, R.S., Pedersen, T.F., Calvert, S.E., Francois, R., 2002. Reduced nitrogen
1220 fixation in the glacial ocean inferred from changes in marine nitrogen and phosphorus
1221 inventories. Nature 415, 156-159.

1222 Garvin, J., Buick, R., Anbar, A. D., Arnold, G.L., Kaufman, A.J., 2009. Isotopic evidence
1223 for an aerobic nitrogen cycle in the latest Archean. Science 323, 1045–1048.

1224 Glasmacher, U.A., Zentilli, M., Ryan, R., 2003. Nitrogen distribution in Lower
1225 Palaeozoic slates/phyllites of the Meguma Supergroup, Nova Scotia, Canada: implications for
1226 Au and Zn–Pb mineralisation and exploration. Chemical Geology 194, 297-329.

1227 Glass, J.B., Wolfe-Simon, F., Elser, J.J., Anbar, A.D., 2010. Molybdenum-nitrogen co-
1228 limitation in freshwater and coastal heterocystous cyanobacteria. Limnology and
1229 Oceanography 55, 667–676.

1230 Glass, J. B., Wolfe-Simon, F., Anbar, A.D., 2009. Coevolution of metal availability and
1231 nitrogen assimilation in cyanobacteria and algae. Geobiology 7, 100–123.

1232 Godfrey, L.V., Falkowski, P.G., 2009. The cycling and redox state of nitrogen in the
1233 Archaean ocean. Nature Geoscience 2, 725–729.

1234 Godfrey, L.V., Glass, J.B., 2011. The geochemical record of the ancient nitrogen cycle,

1235 nitrogen isotopes, and metal cofactors. Methods in Enzymology 486, 483–506.

1236 Godfrey, L.V., Poulton, S.W., Bebout, G.E., Fralick, P.W., 2013. Stability of the nitrogen
1237 cycle during development of sulfidic water in the redox-stratified late Paleoproterozoic ocean.
1238 Geology 41, 655–658.

1239 Goldblatt C., Claire, M.W., Lenton, T.M., Matthews, A.J., Watson, A.J., Zahnle, K.J.,
1240 2009. Nitrogen-enhanced greenhouse warming on early Earth. Nature Geoscience 2, 891-896.

1241 Granger, J., Sigman, D.M., Lehmann, M.F., Tortell, P.D., 2008. Nitrogen and oxygen
1242 isotope fractionation during dissimilatory nitrate reduction by denitrifying bacteria.
1243 Limnology and Oceanography 53, 2533–2545.

1244 Granger, J., Prokopenko, M.G., Sigman, D.M., Mordy, C.W., Morse, Z.M., Morales,
1245 L.V., Sambrotto, R.N., Plessen, B., 2011. Coupled nitrification-denitrification in sediment of
1246 the eastern Bering Sea shelf leads to (15)N enrichment of fixed N in shelf waters. Journal of
1247 Geophysical Research-Oceans, 116.

1248 Griffin, B.M., Schott, J., Schink, B., 2007. Nitrite, an electron donor for anoxygenic
1249 photosynthesis. Science 316, 1870.

1250 Grotzinger, J.P., Kasting, J.F., 1993. New constraints on Precambrian ocean composition.
1251 The Journal of Geology, 235-243.

1252 Gruber, N., Galloway, J.N., 2008. An Earth-system perspective of the global nitrogen
1253 cycle. Nature 451, 293-296.

1254 Hadas, O., Altabet, M.A., Agnihotri, R., 2009. Seasonally varying nitrogen isotope
1255 biogeochemistry of particulate organic matter in Lake Kinneret, Israel. Limnology and
1256 Oceanography 54, 75-85.

1257 Haendel, D., Mühle, K., Nitzsche, H.-M., Stiehl, G., Wand, U., 1986. Isotopic variations

1258 of the fixed nitrogen in metamorphic rocks. Geochimica et Cosmochimica Acta 50, 749-758.

1259 Hayes, J.M., Wedeking, W., Kaplan, I.R., 1983. Precambrian organic geochemistry,
1260 preservation of the record. In: Schopf WJ (ed) Earth's earliest biosphere. Princeton University
1261 Press, Princeton, pp 291-301.

1262
1263 Higgins, M.B., Robinson, R.S., Carter, S.J., Pearson, A., 2010. Evidence from chlorin
1264 nitrogen isotopes for alternating nutrient regimes in the Eastern Mediterranean Sea. Earth and
1265 Planetary Science Letters 290, 102–107.

1266 Higgins, M.B., Wolfe-Simon, F., Robinson, R.S., Qin, Y., Saito, M.A., Pearson, A.,.
1267 2011. Paleoenvironmental implications of taxonomic variation among $\delta^{15}N$ values of
1268 chloropigments. Geochimica Cosmochimica Acta 75, 7351–7363.

1269 Higgins, M.B., Robinson, R.S., Husson, J.M., Carter, S.J., Pearson, A., 2012. Dominant
1270 eukaryotic export production during ocean anoxic events reflects the importance of recycled
1271 NH_4^+. Proceedings of the National Academy of Sciences of the USA 109, 2269-2274.

1272 Hoch, M.P., Fogel, M.L.E., Kirchman, D.L., 1992. Isotopic fractionation associated with
1273 ammonium uptake by marine bacteria. Limnology and Oceanography 3, 1447-1459.

1274 Hoering, T., Ford, H.T., 1960. The isotope effect in the fixation of nitrogen by
1275 Azotobacter. Journal of the American Chemical Society 82, 376– 378.

1276 Holland, H.D., 2006. The oxygenation of the atmosphere and oceans. Philosophical
1277 Transaction of the Royal Society B 361, 903–915.

1278 Jenkyns, H.C., 2010. Geochemistry of oceanic anoxic events, Geochem. Geophys.
1279 Geosyst., 11, Q03004, doi:10.1029/2009GC002788.

1280 Jia, Y., Kerrich, R., 1999. Nitrogen isotope systematics of mesothermal lode gold
1281 deposits: Metamorphic, granitic, meteoric water, or mantle origin? Geology 27, 1051–1054.

1282 Jia, Y., Kerrich, R., 2000. Giant quartz vein systems in accretionary orogenic belts: The
1283 evidence for a metamorphic fluid origin from $\delta^{15}N$ and $\delta^{13}C$ studies. Earth and Planetary
1284 Science Letters 184, 211–224.

1285 Jia, Y., Kerrich, R., 2004a. A reinterpretation of the crustal N-isotope record: Evidence
1286 for a ^{15}N-enriched Archean atmosphere? Terra Nova 16, 102–108.

1287 Jia, Y., Kerrich, R., 2004b. Nitrogen 15-enriched Precambrian kerogen and hydrothermal
1288 systems. Geochemistry, Geophysics, Geosystems 5, 1-21. Q07005,
1289 doi:10.1029/2004GC000716.

1290 Jia, Y., 2006. Nitrogen isotope fractionations during progressive metamorphism: a case
1291 study from the Paleozoic Cooma metasedimentary complex, southeastern Australia.
1292 Geochimica et Cosmochimica Acta 70, 5201-5214.

1293 Junium, C.K., Arthur, M.A., 2007. Nitrogen cycling during the Cretaceous, Cenomanian-
1294 Turonian Oceanic Anoxic Event II. Geochemistry, Geophysics, Geosystems 8, 1-18. Q03002,
1295 doi:03010.01029/02006GC001328.

1296 Junium, C.K., Freeman, K.H., Arthur, M.A., 2014. Controls on the stratigraphic
1297 distribution and nitrogen isotopic composition of zinc, vanadyl and free base porphyrins
1298 through Oceanic Anoxic Event 2 at Demerara Rise, Org. Geochem., 80, 60–71.

1299 Juster, T.C., Brown, P.E., Bailey, S.W., 1987. NH_4-bearing illite in very low grade
1300 metamorphic rocks associated with coal, northeastern Pennsylvania. American Mineralogist,
1301 72, 555-565.

1302 Karl, D., A. Michaels, B. Bergman, D. Capone, E. Carpenter, R. Letelier, F. Lipschultz,
1303 H. Paerl, D. Sigman, Stal, L., 2002. Dinitrogen fixation in the world's oceans.
1304 Biogeochemistry 57-58, 47– 98.

1305 Kemp, A.L.W., Mudrochova, A., 1972. Distribution and forms of nitrogen in a Lake

1306 Ontario sediment core. Limnology and Oceanography 17, 855–867.

1307 Kerrich, R., Jia, Y., Manikyamba, C., Naqvi, S.M., 2006. Secular variations of N-isotopes
1308 in terrestrial reservoirs and ore deposits, in Kesler, S.E., Ohmoto, H., eds., Evolution of Early
1309 Earth's Atmosphere, Hydrosphere, and Biosphere—Constraints from Ore Deposits.
1310 Geological Society of America Memoir 198, 81–104.

1311 Kessler, A.J., Bristow, L.A., Cardenas, M.B., Glud, R.N., Thamdrup, B., Cook, P.L.M.,
1312 2014. The isotope effect of denitrification in permeable sediments. Geochimica et
1313 Cosmochimica Acta 133, 156–167.

1314 Kienast, S.S., Calvert, S.E., Pedersen, T.F., 2002. Nitrogen isotope and productivity
1315 variations along the northeast Pacific margin over the last 120 kyr: Surface and subsurface
1316 paleoceanography. Paleoceanography 17, 1055, doi:1010.1029/2001PA000650.

1317 Knapp, A.N., Sigman, D.M., Lipschultz, F., 2005. N isotopic composition of dissolved
1318 organic nitrogen and nitrate at the Bermuda Atlantic Time-series Study site. Global
1319 Biogeochemal Cycles 19, GB1018, doi:10.1029/2004GB002320.

1320 Konovalov, S.K., Fuchsman, C.A., Belokopitov, V., Murray, J.W., 2008. Modeling the
1321 distribution of nitrogen species and isotopes in the water column of the Black Sea. Marine
1322 Chemistry 111, 106–124.

1323 Kohzu, A., Akio Imai, A., Miyajima, T., Fukushima, T., Matsushige, K., Komatsu, K.,
1324 Kawasaki, N., Miura, S., Sato, T., 2011. Direct evidence for nitrogen isotope discrimination
1325 during sedimentation and early diagenesis in Lake Kasumigaura, Japan. Organic
1326 Geochemistry 42, 173–183.

1327 Kump, L.R., Junium, C., Arthur, M.A., Brasier, A., Fallick, A., Melezhik, V., Lepland,
1328 A., CCrne, A.E., Luo, G., 2011. Isotopic evidence for massive oxidation of organic matter
1329 following the Great Oxidation Event. Science 334, 1694–1696.

1330 Kump, L.R., Pavlov, A., and Arthur, M.A., 2005, Massive release of hydrogen sulfide to
1331 the surface ocean and atmosphere during intervals of oceanic anoxia: Geology 33, 397–400.

1332 Kuypers, M.M., Lavik, G., Woebken, D., Schmid, M., Fuchs, B.M., Amann, R.,
1333 Jørgensen, B.B., Jetten, M.S.M., 2005. Massive nitrogen loss from the Benguela upwelling
1334 system through anaerobic ammonium oxidation. Proceedings of the National Academy of
1335 Science of the USA 102, 6478–6483.

1336 Lam, P., Lavik, G., Jensen, M.M., van de Vossenberg, J., Schmid, M., Woebken, D.,
1337 Dimitri Gutiérrez, D., Amann, R., Jetten, M.S.M., Kuypers, M.M.M., 2009. Revising the
1338 nitrogen cycle in the Peruvian oxygen minimum zone. Proceedings of the National Academy
1339 of Science of the USA 106, 4752–4757.

1340 Lam, P., Kuypers, M.M.M., 2011. Microbial Nitrogen Cycling Processes in Oxygen
1341 Minimum Zones. Marine Science Annual Reviews 3, 317-345.

1342 Lavik, G., Stuhrmann, T., Bruchert, V., Van der Plas, A., Mohrholz, V., Lam, P.,
1343 Muszmann, M., Fuchs, B.M., Amann, R., Lass, U., Kuypers, M.M.M., 2009. Detoxification
1344 of sulphidic African shelf waters by blooming chemolithotrophs. Nature 457, 581-584.

1345 Lehmann, M.F., Bernasconi, S.M., Barbieri, A., McKenzie, J.A., 2002. Preservation of
1346 organic matter and alteration of its carbon and nitrogen isotope composition during simulated
1347 and in situ early sedimentary diagenesis. Geochimica et Cosmochimica Acta 66, 3573-3584.

1348 Lehmann, M.F., Sigman, D.M., Berelson, W.M., 2004. Coupling the N-15/N-14 and O-
1349 18/O-16 of nitrate as a constraint on benthic nitrogen cycling. Marine Chemistry 88, 1–20.

1350 Lehmann, M.F., Sigman, D.M., McCorkle, D.C., Granger, J., Hoffmann, S., Cane, G.,
1351 Brunelle, B.G., 2007. The distribution of nitrate $^{15}N/^{14}N$ in marine sediments and the impact
1352 of benthic nitrogen loss on the isotopic composition of oceanic nitrate. Geochimica et
1353 Cosmochimica Acta 71, 5384-5404.

Lenton, T.M., Boyle, R.A., Poulton, S.W., Shields-Zhou, G.A., Butterfield, N.J., 2014. Co-evolution eukaryotes and ocean oxy- genation in the Neoproterozoic era. Nature Geoscience 7, 257–265.

Letscher, R.T., Hansell, D.A., Carlson, C.A. Lumpkin, R., Knapp, A.N., 2013. Dissolved organic nitrogen in the global surface ocean: Distribution and fate. Global Biogeochemicala Cycles 27, 141–153.

Li, L., Cartigny, P., Ader, M., 2009. Kinetic nitrogen isotope fractionation associated with thermal decomposition of NH_3: experimental results and potential applications to trace the origin of N_2 in natural gas and hydrothermal systems. Geochimica Cosmochimica Acta 73, 6282–6297.

Li, L., Sherwood Lollar, B., Li, H., Wortmann, U.G., Lacrampe-Couloume, G., 2012. Ammonium stability and nitrogen isotope fractionations for NH^+_4-$NH_{3(aq)}$-$NH_{3(gas)}$ systems at 20–70°C and pH of 2–13: Applications to habitability and nitrogen cycling in low-temperature hydrothermal systems. Geochimica et Cosmochimica Acta 84, 280–296.

Libes, S.M., Deuser, W.G., 1988. The isotope geochemistry of particulate nitrogen in the Peru upwelling area and the Gulf of Maine, Deep Sea Research, Part A, 35, 517–533.

Logan, G.A., Hayes, J.M., Hieshima, G.B., Summons, R.E., 1995. Terminal Proterozoic reorganization of biogeochemical cycles. Nature 376, 53–56.

Lyons, T.W., Reinhard, C.T., Planavsky, N.J., 2014. The rise of oxygen in Earth's early ocean and atmosphere. Nature 506, 307–315.

Macko, S.A., Quick, R.S., 1986. A geochemical study of oil migration at source rock reservior contacts: stable isotopes. Organic Geochemistry 10, 199-205.

Macko, S.A., Fogel, M.L., Hare, P.E., Hoering, T.C., 1987, Isotopic fractionation of nitrogen and carbon in the synthesis of amino-acids by microorganisms: Chemical Geology,

65, p. 79–92.

Mandernack, K.W., Mills, C.T., Johnson, C.A., Rahn, T., Kinney, C., 2009. The $\delta^{15}N$ and $\delta^{18}O$ values of N_2O produced during the co-oxidation of ammonia by methanotrophic bacteria. Chemical Geology 267, 96–107.

Mariotti, A., Germon, J.C., Hubert, P., Kaiser, P., Letolle, R., Tardieux, A., Tardieux, P., 1981. Experimental determination of nitrogen kinetic isotope fractionation: some principles; illustration for the denitrification and nitrification processes. Plant Soil 62, 413–430.

Marty, B., Zimmermann, L., Pujol, M., Burgess, R., Philippot, P. 2013. Nitrogen isotopic Composition and density of the Archean atmosphere. Science 342, 101–104.

Meckler, A.N., Haug, G.H., Sigman, D.M., Plessen, B., Petersen, L.C., Thierstein, H.R., 2007. Detailed sedimentary N isotope records from Cariaco Basin for Terminations I and V: local and global implications. Global Biogeochemical Cycles 21, GB4019.

Meyers, P.A., 2006. Paleoceanographic and paleoclimatic similarities between Mediterranean sapropels and Cretaceous black shales. Palaeogeography, Palaeoclimatology, Palaeoecology 235, 305– 320.

Meyers, P.A., Simoneit, B.R.T., 1999. Effects of extreme heating on the elemental and isotopic compositions of an upper Cretaceous coal. Organic Geochemistry 30, 299–305.

Mikhail, S., Sverjensky, D.A., 2014. Nitrogen speciation in upper mantle fluids and the origin of Earth's nitrogen-rich atmosphere. Nature Geoscience 7, 816–819.

Minagawa, M., Wada, E., 1986. Nitrogen isotope ratios of the red tide organisms in the East China Sea: A characterization of biological nitrogen fixation. Marine Chemistry 19, 245–259.

Mingram, B., Bräuer, K., 2001. Ammonium concentration and nitrogen isotope

composition in metasedimentary rocks from different tectonometamorphic units of the European Variscan Belt. Geochimica et Cosmochimica Acta 65, 273-287.

Mingram, B., Hoth, P., Lüders, V., Harlov, D.E., 2005. The significance of fixed ammonium in Palaeozoic sediments for the generation of nitrogen-rich natural gases in the North German Basin. International Journal of Earth Science 94, 1010–1022.

Möbius, J., Lahajnar, N., Emeis, K.C., 2010. Diagenetic control of nitrogen isotope ratios in Holocene sapropels and recent sediments from the Eastern Mediterranean Sea. Biogeosciences 7, 3901-3914.

Möbius, J., Gaye, B., Lahajnar, N., Bahlmann, E., Emeis, K.C., 2011. Influence of diagenesis on sedimentary $\delta^{15}N$ in the Arabian Sea over the last 130 kyr. Marine Geology 284, 127–138.

Möbius, J., 2013. Isotope fractionation during nitrogen remineralization (ammonification): Implications for nitrogen isotope biogeochemistry. Geochimica et Cosmochimica Acta 105, 422–432.

Moine, B., Guillot, C., Gibert, F. 1994. Controls of the composition of nitrogen-rich fluids originating fromreaction with graphite and ammonium-bearing biotite. Geochimica et Cosmochimica Acta 58, 5503–5523.

Moodley, L., Middleburg, J.J., Herman, P.M.J., Soetaert, K., de Lange, G.J., 2005. Oxygenation and organic-matter preservation in marine sediments: direct experimental evidence from ancient organic carbon–rich deposits. Geology 33, 889–892.

Moore, C.M., Mills, M.M., Arrigo, K.R., Berman-Frank, I., Bopp, L., Boyd, P.W., Galbraith, E.D., Geider, R.J., Guieu, C., Jaccard, S.L., Jickells, T.D., La Roche, J., Lenton, T.M., Mahowald, N.M., Marañón, E., Marinov, I., Moore, J.K., Nakatsuka, T., Oschlies, A.,

1424 Saito, M.A., Thingstad, T.F., Tsuda A., Ulloa, O., 2013. Processes and patterns of oceanic
1425 nutrient limitation. Nature Geoscience 6, 701–710.

1426 Müller, P.J., 1977. C–N ratios in Pacific deep-sea sediments – effect of inorganic
1427 ammonium and organic nitrogen-compounds sorbed by clays. Geochimica et Cosmochimica
1428 Acta 41, 765–776.

1429 Nakanishi, T., Minagawa, M., 2003. Stable carbon and nitrogen isotopic compositions of
1430 sinking particles in the northeast Japan Sea. Geochemical Journal, 37, 261-275.

1431 Nishizawa, M., Sano, Y., Ueno, Y., Maruyama, S., 2007. Speciation and isotope ratios of
1432 nitrogen in fluid inclusions from seafloor hydrothermal deposits at ~3.5Ga. Earth and
1433 Planetary Science Letters 254, 332–344.

1434 Och, L.M., Shields-Zhou, G.A., 2012. The Neoproterozoic oxygenation event:
1435 Environmental perturbations and biogeochemical cycling. Earth-Science Reviews 110, 26-57.

1436 Oehler, D.Z., Robert, F., Walter, M.R., Sugitani, K., Meiborn, A., Mostefaoui, S.,
1437 Gibson, E.K., 2010. Diversity in the Archean biosphere: new insights from NanoSIMS.
1438 Astrobiology 10, 413-424.

1439 Oehler, D.Z., Robert, F., Walter, M.R., Sugitani, K., Allwood, A., Meibom, A.,
1440 Mostefaoui, S., Selo, M.R., Thomen, A., Gibson, E.K., 2009. NANOSIMS: insights to
1441 biogenicity and syngeneity of Archaean carbonaceous structures. Precambrian Research 173,
1442 70–78.

1443 Oehler, D.Z., Robert, F., Mostefaoui, S., Meibom, A., Selo, M., McKay, D.S., 2006.
1444 Chemical mapping of Proterozoic organic matter at sub-micron spatial resolution.
1445 Astrobiology 6, 838–850.

1446 Olson, J.M., 1970. The evolution of photosynthesis. Science 168, 438–446.

1447 Palya, A.P., Buick, I.S., Bebout, G.E., 2011. Storage and mobility of nitrogen in the
1448 continental crust: Evidence from partially melted metasedimentary rocks, Mt. Stafford,
1449 Australia. Chemical Geology 281, 211-226.

1450 Papineau, D., Mojzsis, S.J., Karhu, J.A., Marty, B., 2005. Nitrogen isotopic composition
1451 of ammoniated phyllosilicates: case studies from Precambrian metamorphosed sedimentary
1452 rocks. Chemical Geology 216, 37-58.

1453 Papineau, D., Purohit, R., Goldberg, T., Pi, D., Shields, G.A., Bhu, H., Steele, A., Fogel,
1454 M.L., 2009. High primary productivity and nitrogen cycling after the Paleoproterozoic
1455 phosphogenic event in the Aravalli Supergroup, India. Precambrian Research 171, 37-56.

1456 Papineau, D., DeGregorio, B.T., Stroud, R.M., Steele, A., Pecoits, E., Konhauser, K.,
1457 Wang, J., Fogel, M.L., 2010. Ancient graphite in the Eoarchean quartz-pyroxene rock from
1458 Akilia in southern West Greenland II: Isotopic and chemical compositions and comparison
1459 with Paleoproterozoic banded iron formations. Geochimica et Cosmochimica Acta 74, 5884-
1460 5905.

1461 Papineau, D., Purohit, R., Fogel, M.L., Shields-Zhou, G.A., 2013. High phosphate
1462 availability as a possible cause for massive cyanobacterial production of oxygen in the
1463 Paleoproterozoic atmosphere. Earth and Planetary Science Letters 362, 225–236.

1464 Papineau, D., De Gregorio, B.T., Fearn, S, Kilcoyne, D., Purohit, R., Fogel, M.L. 2016.
1465 Nanoscale petrographic and geochemical insights on the origin of Paleoproterozoic
1466 stromatolitic phosphorites from Aravalli, India. Geobiology 14, 3-32.

1467 Partin, C.A., Bekker, A., Planavsky, N.J., Scott, C.T., Gill, B.C., Li, C., Podkovyrov, V.,
1468 Maslov, A., Konhauser, K.O., Lalonde, S.V., Love, G.D., Poulton, S.W., Lyons, T.W., 2013.
1469 Large-scale fluctuations in Precambrian atmospheric and oceanic oxygen levels from the
1470 record of U in shales. Earth and Planetary Science Letters 369–370, 284–293.

Pennock, J.R., Velinsky, D.J., Ludlam, J.M., Sharp, J.H., Fogel, M.L., 1996. Isotopic fractionation of ammonium and nitrate during uptake by Skeletonema costatum: implications for $\delta^{15}N$ dynamics under bloom conditions. Limnology and Oceanography 41, 451–459.

Peters, K.E., Sweeney, R.E., Kaplan, I.R.,1978. Correlation of carbon and nitrogen stable isotope ratios in sedimentary organic matter. Limnology and Oceanography 23, 598-604.

Pinti, D.L., Hashizume, K., Matsuda, J., 2001. Nitrogen and argon signatures in 3.8–2.8 Ga metasediments: clues on the chemical state of the Archean ocean and the deep biosphere. Geochimica et Cosmochimica Acta 65, 2301–2315.

Pinti, D.L., Hashizume, K., 2001. ^{15}N-depleted nitrogen in Early Archean kerogens: clues on ancient marine chemosynthetic-based ecosystems? A comment to Beaumont, V., Robert, F., 1999. Precambrian Res. 96, 62–82. Precambrian Research 105, 85–88.

Pinti D. L., Hashizume K., Orberger B., Gallien J. -P., Cloquet C., Massault M., 2007. Biogenic nitrogen and carbon in Fe-Mn-oxyhydroxides from an Archean chert, Marble Bar, Western Australia. Geochemistry, Geophysics, Geosystems 8, doi:10.1029/2006GC001394.

Pinti, D.L., Hashizume, K. Sugihara, A., Massault, M., Philippot, P., 2009. Isotopic fractionation of nitrogen and carbon in Paleoarchean cherts from Pilbara craton, Western Australia: Origin of ^{15}N-depleted nitrogen. Geochimica et Cosmochimica Acta 73, 3819–3848.

Pinti, D.L., Hashizume, K., 2011. Early life recorded by nitrogen isotopes. In: (Golding, S., Glikson, M., eds) Earliest Life on Earth: Habitats, Environments and Methods of Detection, Springer-Verlag, Berlin, 183-205.

Pitcairn, I.K., Teagle, D.A.H., Kerrich, R., Craw, D., Brewerd, T.S., 2005. The behavior of nitrogen and nitrogen isotopes during metamorphism and mineralization: evidence from

1494 the Otago and Alpine Schists, New Zealand. Earth and Planetary Science Letters 233, 229–
1495 246.

1496 Plessen, B., Harlov, D.E., Henry, D., Guidotti, C.V., 2010. Ammonium loss and nitrogen
1497 isotopic fractionation in biotite as a function of metamorphic grade in metapelites from
1498 western Maine, USA. Geochimica et Cosmochimica Acta 74, 4759-4771.

1499 Polissar, P.J., Fulton, J.M., Juniun, C.K., Turich, C.C., Freeman, K.H., 2008.
1500 Measurement of ^{13}C and ^{15}N isotopic composition on nanomolar quantities of C and N.
1501 Analytical Chemistry 81, 755–763.

1502 Poulton, S.W., Canfield, D.E., 2011. Ferruginous conditions: a dominant feature of the
1503 Ocean through Earth's history. Elements 7, 107–112.

1504 Prahl, F.G., Cowie, GL., De Lange, G.J., Sparrow, M.A., 2003. Selective organic matter
1505 preservation in ''burn-down'' turbidites on the Madeira Abyssal Plain. Paleoceanography 18,
1506 1052–1065.

1507 Pride, C., Thunell, R., Sigman, D., Keigwin, L., Altabet, M., Tappa, E., 1999. Nitrogen
1508 isotopic variations in the Gulf of California since the last deglaciation: response to global
1509 climate change. Paleoceanography 14 , 397– 409.

1510 Prokopenko, M.G., Hammond, D.E., Berelson, W.M., Bernhard, J.M., Stott, L., Douglas,
1511 R., 2006a. Nitrogen cycling in the sediments of Santa Barbara Basin and Eastern Tropical
1512 North Pacific: nitrogen isotopes, diagenesis and possible chemosymbiosis between two
1513 lithotrophs (Thioploca and Anammox)—''riding on a glider''. Earth and Planetary Science
1514 Letters 242, 186-204.

1515 Prokopenko, M.G., Hammond, D.G., Spivack, A., Stott, L., 2006b. 5. Impact of long-
1516 term diagenesis on $\delta^{15}N$ of organic matter in marine sediments : sites 1227 and 1230. In
1517 Proceedings of the Ocean Drilling Program, Scientific Results (eds. B. B. Jorgensen, S. L.

1518 D'Hondt and D. J. Miller). College Station, TX (Ocean Drilling Program).

1519 Prokopenko, M.G., Hammond, D.E., Stott, L., 2006c. Lack of isotopic fractionation of
1520 $\delta^{15}N$ of organic matter during long-term diagenesis in marine sediments, ODP leg 202, sites
1521 1234 and 1235. In Proceedings of the Ocean Drilling Program, Scientific Results (eds. R.
1522 Tiedemann, A. C. Mix, C. Richter and W. F. Ruddiman). College Station, TX (Ocean Drilling
1523 Program).

1524 Prokopenko, M.G., Hirst, M.B., De Brabandere, L., Lawrence, D.J.P., Berelson, W.M.,
1525 Granger, J., Chang, B.X., Dawson, S., Crane III, E.J., Chong, L., Thamdrup, B., Townsend-
1526 Small, A., Sigman, D.M., 2013. Nitrogen losses in anoxic marine sediments driven by
1527 Thioploca–anammox bacterial consortia. Nature 500, 194-198.

1528 Quan, T.M., Falkowski, P.G., 2009. Redox control of N:P ratios in aquatic ecosystems.
1529 Geobiology 7, 124–139.

1530 Quan, T.M., Wright, J.D., Falkowski, P.G., 2013. Covariation of nitrogen isotopes and
1531 redox states through glacial–interglacial cycles in the Black Sea. Geochimica et
1532 Cosmochimica Acta 112, 305–320.

1533 Reinhard, C.T., Planavsky, N.J., Robbins, L.J., Partin, C.A., Gill, B.C., Lalonde, S.V.,
1534 Bekker, A., Konhauser, K.O., Lyons, T.W., 2013. Proterozoic ocean redox and
1535 biogeochemical stasis. Proceedings of the National Academy of Science of the USA 110,
1536 5357–5362.

1537 Rivera, K.T., Puckette, J., Quan, T.M., 2015. Evaluation of redox versus thermal maturity
1538 controls on $\delta^{15}N$ in organic rich shales: A case study of the Woodford Shale, Anadarko Basin,
1539 Oklahoma, USA. Organic Chemistry 83-84, 127-139.

1540 Roberson, L., Roadt, J., Halevy, I., Kasting, J.F., 2011. Greenhouse warming by nitrous
1541 oxide and methane in the Proterozoic Eon. Geobiology 9, 313–320.

Robinson, R.S., Kienast, M., Luiza Albuquerque, A., Altabet, M., Contreras, S., De Pol Holz, R., Dubois, N., Francois, R., Galbraith, E., Hsu, T.C., Ivanochko, T., Jaccard, S., Kao, S.J., Kiefer, T., Kienast, S., Lehmann, M., Martinez, P., McCarthy, M., Möbius, J., Pedersen, T., Quan, T.M., Ryabenko, E., Schmittner, A., Schneider, R., Schneider-Mor, A., Shigemitsu, M., Sinclair, D., Somes, C., Studer, A., Thunell, R., Yang, J.Y., 2012. A review of nitrogen isotopic alteration in marine sediments. Paleoceanography 27, PA4203.

Sachs, J.P., Repeta, D.J., 1999. Oligotrophy and nitrogen fixation during Eastern Mediterranean sapropel events. Science 286, 2485–2488.

Sachs, J. P., Repeta, D. J., Goericke, R., 1999. Nitrogen and carbon isotopic ratios of chlorophyll from marine phytoplankton, Geochimica et Cosmochimica Acta 63, 1431-1441.

Saito, M.A., Sigman, D.M., Morel, F.M.M., 2003. The bioinorganic chemistry of the ancient ocean: the co-evolution of cyanobacterial metal requirements and biogeochemical cycles at the Archean-Proterozoic boundary? Inorganica Chimica Acta 356, 308-318.

Sánchez-Baracaldo, P., Ridgwell, A., Raven, J.A., 2014. A Neoproterozoic transition in the marine nitrogen cycle. Current Biology 24, 652-657.

Sano, Y., Pillinger, C.T., 1990. Nitrogen isotopes and N_2/Ar ratios in cherts: an attempt to measure time evolution of atmospheric $\delta^{15}N$ value. Geochemistry Journal 24, 315–324.

Santoro, A.E., Casciotti, K.L., 2011. Enrichment and characterization of ammonia oxidizing archaea from the open ocean: phylogeny, physiology and stable isotope fractionation. ISME J. 5, 1796–1808.

Schimmelmann, A., Lis, G.P., 2010. Nitrogen isotopic exchange during maturation of organic matter. Organic Geochemistry 41, 63-70.

Schimmelmann, A., Mastalerz, M., Gao, L., Sauer, P.E., Topalov, K., 2009. Dike intrusions into bituminous coal, Illinois Basin: H, C, N, O isotopic responses to intermittent

heating. Geochimica et Cosmochimica Acta 73, 6264–6281.

Schott, J., Griffin, B.M., Schink, B., 2010. Anaerobic phototrophic nitrite oxidation by Thiocapsa sp. strain KS1 and Rhodopseudomonas sp. strain LQ17. Microbiology 156, 2428–2437.

Schubert, C.J., Calvert, S.E., 2001, Nitrogen and carbon isotopic composition of marine and terrestrial organic matter in Arctic Ocean sediments: implications for nutrient utilization and organic matter composition: Deep Sea Research Part I: Oceanographic Research Papers 48, 789-810.

Sephton, A., Verchovsky, A.B., Bland, P.A., Gilmour, I., Grady, M.M., Wright, I.P., 2003. Investigating the variations in carbon and nitrogen isotopes in carbonaceous chondrites. Geochimica et Cosmochimica Acta 67, 2093–2108.

Sigman, D.M., Karsh, K.L., Casciotti, K.L., 2009. Nitrogen isotopes in the ocean, in: Steele, J.H., Thorpe, S.A., Turekian, K.K. (Eds) Encyclopedia of Ocean Sciences. Academic Press, Oxford, pp. 40–54.

Sohm, J.A., Webb, E.A., Capone, D.G., 2011, Emerging patterns of marine nitrogen fixation. Nature Reviews Microbiology 9, 499-508.

Somes, C.J., Schmittner, A., Galbraith, E.D., Lehmann, M.F., Altabet, M.A., Montoya, J.P., Letelier, R.M., Mix, A.C., Bourbonnais, A., Eby, M., 2010. Simulating the global distribution of nitrogen isotopes in the ocean. Global Biogeochemical Cycles 24, GB4019.

Sperling, E.A., Roonay, A.D., Hays, L., Sergeev, V.N., Vorob'eva, N.G., Sergeev, N.D., Selby, D., Johnston, D.T., Knoll, A.H., 2014. Redox heterogeneity of subsurface waters in the Mesoproterozoic ocean. Geobiology 12, 373-386.

1588 Straub, M., Sigman, D.M., Ren, H., Martinez-Garcia, A., Meckler, A.N., Hain, M.P.,
1589 Haug, G.H., 2013. Changes in North Atlantic nitrogen fixation controlled by ocean
1590 circulation. Nature 501, 200-203.

1591 Sterne, E.J., Reynolds, R.C., Zantop, Jr.H., 1982. Natural ammonium illites from black
1592 shales hosting a stratiform base metal deposit, Delong Mountains, Northen Alaska. Clays and
1593 Clay Minerals 30, 161-166.

1594 Stüeken, E.E., 2013. A test of the nitrogen-limitation hypothesis for retarded eukaryote
1595 radiation: nitrogen isotopes across a Mesoproterozoic basinal profile. Geochimica et
1596 Cosmochimica Acta 120, 121-139.

1597 Stüeken, E.E., Buick, R., Guy, B.M., Koehler, M.C., 2015a. Isotopic evidence for
1598 biological nitrogen fixation by molybdenum-nitrogenase from 3.2Gyr. Nature 520, 666–669.

1599 Stüeken, E.E., Buick, R., Schauer, A.J., 2015b. Nitrogen isotope evidence for alkaline
1600 lakes on late Archean continents. Earth and Planetary Science Letters 411, 1–10.

1601 Sucha, V., Kraus, I., Madejova, J., 1994. Ammonium illite from anchimetamorphic
1602 shales associated with anthracite in the Zemplinicum of the western Carpathians. Clay
1603 Minerals 29, 369-377.

1604 Svensen, H., Bebout, G., Kronz, A., Li, L., Planke, S., Chevallier, L., Jamtveit, B., 2008.
1605 Nitrogen gechemistry as a tracer of fluid flow in a hydrothermal vent complex in the Karoo
1606 Basin, South Africa. Geochimica et Cosmochimica Acta 72, 4929-4947.

1607 Tesdal, J.E., Galbraith, E.D., Kienast, M., 2013. Nitrogen isotopes in bulk marine
1608 sediment: linking seafloor observations with subseafloor records. Biogeosciences 10, 101-
1609 118.

Teske, A., Alm, E., Regan, J.M., Toze, S., Rittmann, B.E., Stahl, D.A., 1994. Evolutionary Relationships among Ammonia- and Nitrite-Oxidizing Bacteria. Journal of Bacteriology 176, 6623-6630.

Thomazo, C., Pinti, D.L., Busigny, V., Ader, M., Hashizume, K., Philippot, P., 2009. Biological activity and the Earth's surface evolution: Insights from carbon, sulfur, nitrogen and iron stable isotopes in the rock record. Comptes Rendus Palevol 8, 665-678.

Thomazo, C., Ader, M., Philippot, P., 2011. Extreme ^{15}N-enrichment in 2.72-Gyr-old sediments: evidence for a turning point in the nitrogen cycle. Geobiology 9, 107–120.

Thomazo, C., Papineau, D., 2013. Biogeochemical cycling of nitrogen on the early Earth. Elements 9, 345–351.

Thunell, R.C., Sigman, D.M., Muller-Karger, F., Astor, Y., Varela, R., 2004. Nitrogen isotope dynamics of the Cariaco Basin, Venezuela. Global Biogeochemical Cycles 18, GB3001, doi:3010.1029/2003GB002185.

Thunell, R., Kepple, A., 2004. Glacial-Holocene nitrogen isotope record from the Gulf of Tehuantepec, Mexico: Implications for denitrification in the eastern equatorial Pacific and changes in atmospheric N_2O. Global Biogeochemical Cycles 18, GB1001, doi:10.1029/2002GB002028.

Tribovillard, N., Algeo, T.J., Baudin, F., Riboulleau, A., 2013. Analysis of marine environmental conditions based on molybdenum–uranium covariation—Applications to Mesozoic paleoceanography. Chemical Geology 324-325, 46–58.

Tyler, T., Kashiyama, Y., Ohkouchi, N., Ogawa, N., Yokoyama, Y., Chikaraishi, Y., Staff, R.A., Ikehara, M., Bronk Ramsey, C., Bryant, C., Brock, F., Gotanda, K., Haraguchi, T., Yonenobu, H., Nakagawa, T., 2010. Tracking aquatic change using chlorin-specific carbon and nitrogen isotopes: The last glacial interglacial transition at Lake Suigetsu, Japan,

1634 Geochem. Geophys. Geosyst., 11, Q09010, doi:10.1029/2010GC003186.

1635 Tyrrell, T., 1999. The relative influences of nitrogen and phosphorus on oceanic primary
1636 production. Nature 400, 525-531.

1637 Van Zuilen, M.A., Mathew, K., Wopenka, B., Lepland, A., Marti, K., Arrhenius, G.,
1638 2005. Nitrogen and argon isotopic signatures in graphite from the 3.8-Ga-old Isua
1639 Supracrustal Belt, Southern West Greenland. Geochimica et Cosmochimica Acta 69, 1241-
1640 1252.

1641 Velinsky, D.J., Fogel, M.L., Todd, J.F., Tebo, B.M., 1991. Isotopic fractionation of
1642 dissolved ammonium at the oxygen-hydrogen sulfide interface in anoxic waters. Geophysical
1643 Research Letters 18, 649-652.

1644 Vo, J., Inwood, W., Hayes, J.M., Kustu, S., 2013. Mechanism for nitrogen isotope
1645 fractionation during ammonium assimilation by Escherichia coli K12. Proceedings of the
1646 National Academy of Sciences of the USA 110, 8696–8701.

1647 Volkova, I.B., Bogdanova, M.V., 1989. Properties of high-rank coals and dispersed
1648 organic matter of associated rocks in the Donets Basin (U.S.S.R.). International Journal of
1649 Coal Geology 11, 315–339.

1650 Voss, M., Nausch, G., Montoya, J.P., 1997. Nitrogen stable isotope dynamics in the
1651 central Baltic Sea: influence of deep-water renewal on the N-cycle changes. Marine Ecology
1652 Progress Series 158,11-21.

1653 Voss, M., Dippner, J.W., Montoya, J.P., 2001. Nitrogen isotope patterns in the oxygen-
1654 deficient waters of the Eastern Tropical North Pacific Ocean. Deep Sea Research Part I:
1655 Oceanographic Research Papers 48, 1905-1921.

1656 Wacey, D., McLoughlin, N., Kilburn, M.R., Saunders, M., Cliff, J.B., Kong, C., Barley,
1657 M.E., Brasier, M.D., 2013. Nanoscale analysis of pyritized microfossils reveals differential

heterotrophic consumption in the 1.9 Ga Gunflint chert. Proceedings of the National Academy of Sciences of the USA 110, 8020-8024.

Wacey, D., Saunders, M., Cliff, J., Kilburn, M.R., Kong, C., Barley, M.E., Brasier, M.D., 2014. Geochemistry and nano-structure of a putative 3240 million-year-old black smoker biota, Sulphur Springs Group, Western Australia. Precambrian Research 249, 1-12.

Wacey, D., Kilburn, M.R. Saunders, Cliff, J.B., Kong, C., Liu, A.G., Matthews, J.J., Brasier, M.D., 2015. Uncovering frmaboidal pyrite biogenecity using nano-scale CN_{org} mapping. Geology 43, 27-30.

Wenk, C.B., Blees, J., Zopfi, J., Veronesi, M.L., Bourbonnais, A., Schubert, C.J., Niemann, H., Lehmann, M.F., 2013. Anaerobic ammonium oxidation (anammox) bacteria and sulfide-dependent denitrifiers coexist in the water column of a meromictic south-alpine lake. Limnology and Oceanography 58, 1–12.

Wenk, C.B., Zopfi, J., Blees, J., Veronesi, M., Niemann, H., Lehmann, M.F., 2014. Community N and O isotope fractionation by sulfide-dependent denitrification and anammox in a stratified lacustrine water column. Geochimica et Cosmochimica Acta 125, 551–563

Westley, M.B., Yamagishi, H., Popp B.N., Yoshida, N., 2006. Nitrous oxide cycling in the Black Sea inferred fromstable isotope and isotopomer distributions. Deep-Sea Research Part II, Topical Studies in Oceanography 53, 1802–1816

Whiticar, M.J., 1996. Stable isotopes geochemistry of coals, humic kerogens and related natural gases. International Journal of Coal Geology 32, 191–215.

Williams, L.B., Ferrell, R.E., Hutcheon, I., Bakel, A.J., Walsh, M.M., Krouse, H.R., 1995. Nitrogen isotope geochemistry of organic matter and minerals during diagenesis and hydrocarbon migration. Geochimica et Cosmochimica Acta 59, 765-779.

Wright, I.P., Boyd, S.R., Franchi, I.A., Pillinger, C. T., 1988. High-precision

1682 determination of nitrogen stable isotope ratios at the sub-nanomole level. Journal of Physics
1683 E: Science Instruments 21, 865–875.

1684 Yamaguchi, K.E., 2002. Geochemistry of Archean–Paleoproterozoic Black Shales: the
1685 Early Evolution of The Atmosphere, Oceans, and Biosphere. PhD, Pennsylvania State
1686 University, 485pp.

1687 Yamaguchi, K.E., Oguri, K., Ogawa, N.O., Sakai, S., Hirano, S., Kitazato, H., Ohkouchi,
1688 N., 2010. Geochemistry of modern carbonaceous sediments overlain by a water mass showing
1689 photic zone anoxia in the saline meromictic Lake Kai-ike, southwest Japan: I. Early
1690 diagenesis of organic carbon, nitrogen, and phosphorus. Palaeogeography Palaeoclimatology
1691 Palaeoecology 294, 72-82.

1692 Yui, T.F., Kao, S.J., Wu, T.W., 2009. Nitrogen and N-isotope variation during low-grade
1693 metamorphism of the Taiwan mountain belt. Geochemical Journal 43, 15-27.

1694 Zerkle, A., Junium, C.K., Canfield, D.E., House, C.H. 2008. Production of ^{15}N-depleted
1695 biomass during cyanobacterial N_2-fixation at high Fe concentrations. Journal of Geophysical
1696 Research 113, http://dx.doi.org/10.1029/2007JG000651.

1697 Zhang, D., 1988. Nitrogen concentrations and isotopic compositions of some terrestrial
1698 rocks. PhD, The University of Chicago.

1699 Zhang, X., Sigman, D.M., Morel, F.M., Kraepiel, A.M., 2014. Nitrogen isotope
1700 fractionation by alternative nitrogenases and past ocean anoxia. Proceedings of the National
1701 Academy of Sciences of the USA 111, 4782-4787.

1702

1703 **Figure Caption**

1704

Figure 1: Succession of conditions and assumptions needed to interpret $\delta^{15}N_{sed}$ measurements in Precambrian sedimentary rocks in terms of N biogeochemical cycle.

Figure 2: $\delta^{15}N_{ker}$ as a function of $\delta^{15}N_{bulk}$ for samples for which paired data are available. Zaonega Fm. (Kump et al., 2011); Campbellrand-Malmani platform (Godfrey et al., 2009); Animikie Bain shelf (Godfrey et al., 2013); Soanesville group and Witwatersand Supergroup (Stüeken et al., 2015a); Tumbiana and Kylena Fms. (Stüeken et al., 2015b); see also the data compilation in the supplementary material.

Figure 3: Schematic diagram of the principal biogeochemical processes driving the modern N cycle adapted from Thomazo et al. (2011). Nitrogen isotope fractionations ($\varepsilon_{reactant\text{-}\ product} \sim \delta_{reactant} - \delta_{product}$) are from the compilations of Cascioti et al. (2009) and Sigman et al. (2009), updated with later publications (Zerkle et al., 2008; Bruner et al., 2013; Mobius, 2013; Zhang et al., 2014).

Figure 4: Simplified representation of the N biogeochemical cycle in putative Precambrian ocean redox structures and of their expected N isotope signature in marine sediments. The red color indicates anoxic waters, the blue color oxygenated waters. $\varepsilon_{ap} \approx 0‰$ indicates cases where the reaction is complete so that the apparent isotope fractionation (ε_{ap}) is close to nil. (a) Modern-like oxic ocean scenario: denitrification does not reach completion (NO_3^- is not quantitatively reduced) in the core of nitrogenous OMZs and O_2 penetrates into surface sediments except where the seafloor intersects an OMZ. (b) Oxic ocean scenario where NO_3^- is quantitatively lost in the core of euxinic OMZs and O_2 rarely penetrates surface sediments.

(c) Physically and redox-stratified ocean scenario: within the redox transition zone downward diffusing NO_3^- and upward diffusing NH_4^+ are quantitatively converted to N_2/N_2O so that hardly any bioavailable-N is supplied to surface waters. (d) Convecting redox-stratified ocean scenario with a relatively deep redox transition zone: NO_3^- and NH_4^+ are quantitatively converted to N_2/N_2O at the redox transition zone, except at upwelling locations where NH_4^+ upwelled in the oxygenated surface waters is concurrently oxidized to NO_3^- and N_2/N_2O. (e) Convecting redox-stratified ocean scenario with a shallow redox transition zone: in upwelling zones anoxic waters reach the surface allowing NH_4^+ to be assimilated and possibly oxidized to N_2 and N_2O. (f) Convecting fully-anoxic ocean scenario: NH_4^+ is assimilated and possibly oxidized to N_2 and N_2O. Modified and completed after Ader et al. (2014).

Figure 5: Histograms for: (a) $\delta^{15}N_{bulk}$ frequency for modern sediments (after Tesdal et al., 2013); (b) median $\delta^{15}N_{sed}$ value of Phanerozoic sedimentary units (median $\delta^{15}N_{sed}$ are from Algeo et al., 2014) (c) $\delta^{15}N_{sed}$ values for OAEs (references in Ader et al., 2014); $\delta^{15}N_{bulk}$ and $\delta^{15}N_{ker}$ value for (d) the Precambrian and for the time intervals (e) 680 to 540 Ma (f) 2.2 to 1.8 Ga (g) 2.8 to 2.4 Ga and (h) 3.8 to 2.8 Ga.

Figure 6: Sedimentary $\delta^{15}N_{bulk}$ and $\delta^{15}N_{ker}$ data plotted versus time. Data and their references are provided in the supplementary material. GOE stands for the Great Oxidation Event.

Figure

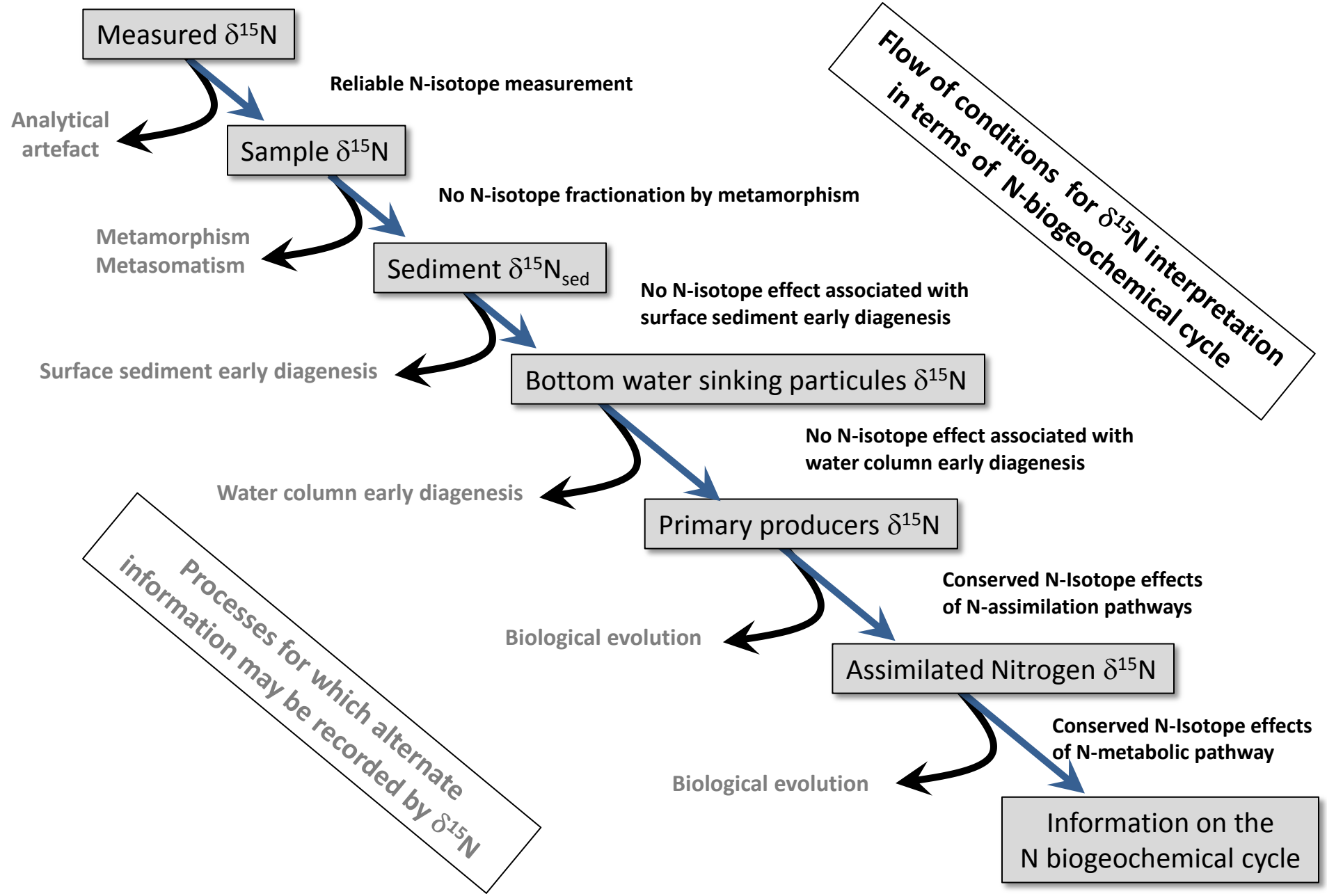
Measured δ15N
Reliable N-isotope measurement
Analytical artefact
Sample δ15N
No N-isotope fractionation by metamorphism
Metamorphism Metasomatism
Sediment δ15Nsed
No N-isotope effect associated with surface sediment early diagenesis
Surface sediment early diagenesis
Bottom water sinking particules δ15N
No N-isotope effect associated with water column early diagenesis
Water column early diagenesis
Primary producers δ15N
Conserved N-Isotope effects of N-assimilation pathways
Biological evolution
Assimilated Nitrogen δ15N
Conserved N-Isotope effects of N-metabolic pathway
Biological evolution
Information on the N biogeochemical cycle
Flow of conditions for δ15N interpretation in terms of N-biogeochemical cycle
Processes for which alternate information may be recorded by δ15N

Figure

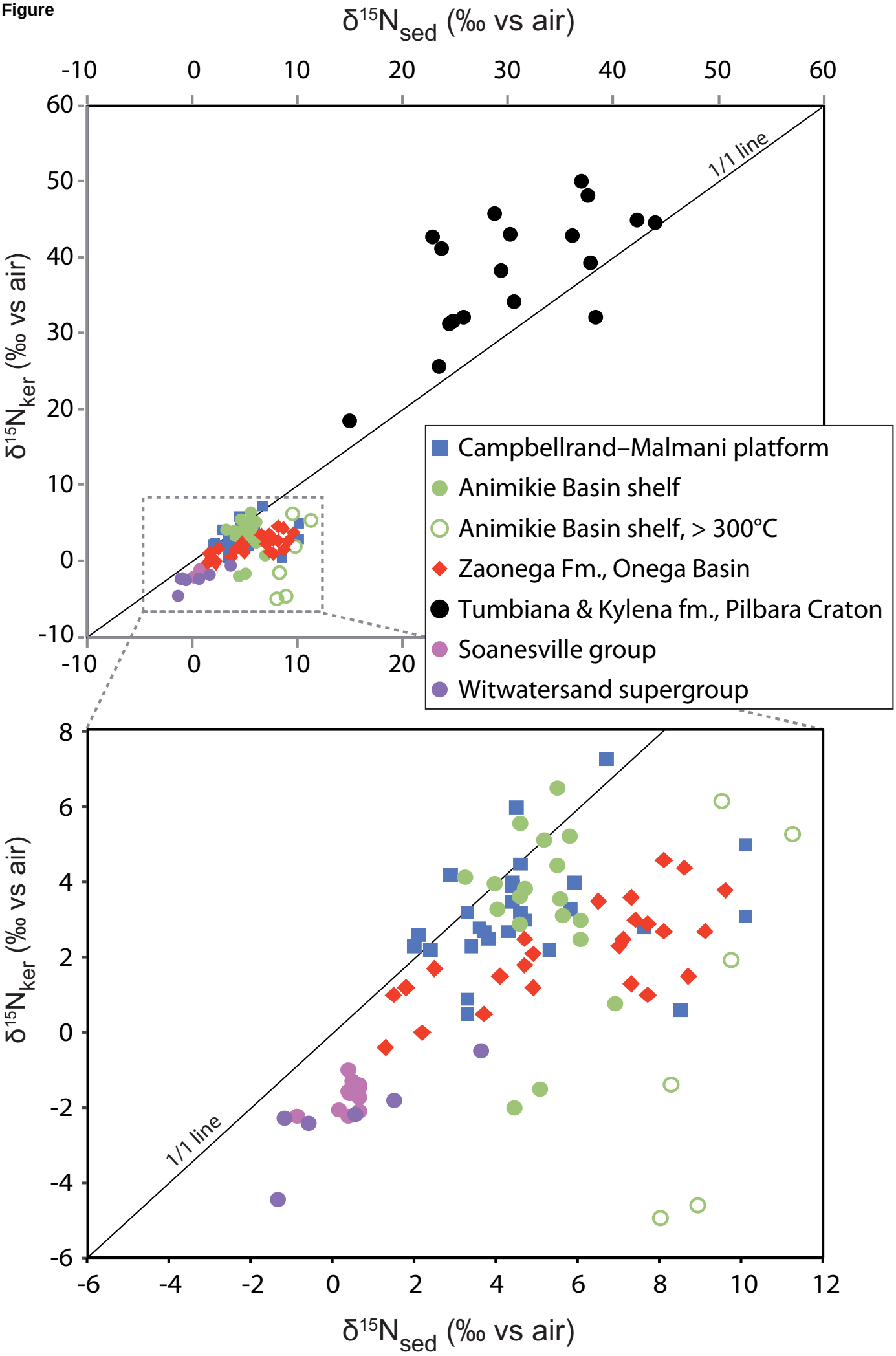
δ15Nsed (‰ vs air)
δ15Nker (‰ vs air)
1/1 line
Campbellrand–Malmani platform
Animikie Basin shelf
Animikie Basin shelf, > 300°C
Zaonega Fm., Onega Basin
Tumbiana & Kylena fm., Pilbara Craton
Soanesville group
Witwatersand supergroup

Figure

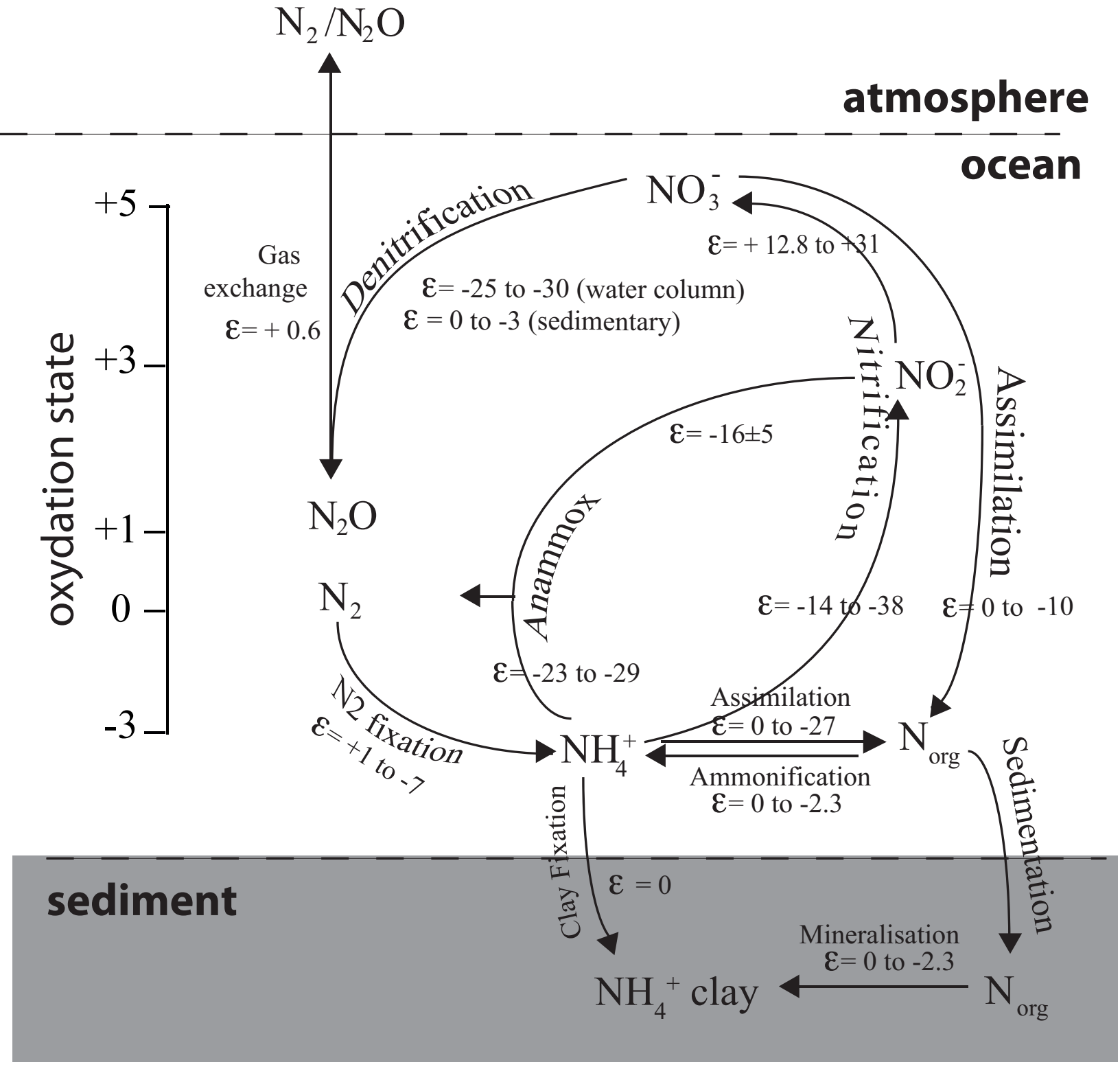
N_2/N_2O
atmosphere
ocean
+5
+3
+1
0
-3
oxydation state
Gas exchange
ε= + 0.6
Denitrification
NO_3^-
ε= + 12.8 to +31
ε= -25 to -30 (water column)
ε = 0 to -3 (sedimentary)
Nitrification
NO_2^-
Assimilation
ε= -16±5
N_2O
Anammox
N_2
ε= -14 to -38
ε= 0 to -10
ε= -23 to -29
N2 fixation
ε= +1 to -7
Assimilation
ε= 0 to -27
NH_4^+
N_{org}
Ammonification
ε= 0 to -2.3
Sedimentation
Clay Fixation
ε = 0
sediment
Mineralisation
ε= 0 to -2.3
NH_4^+ clay
N_{org}

Figure

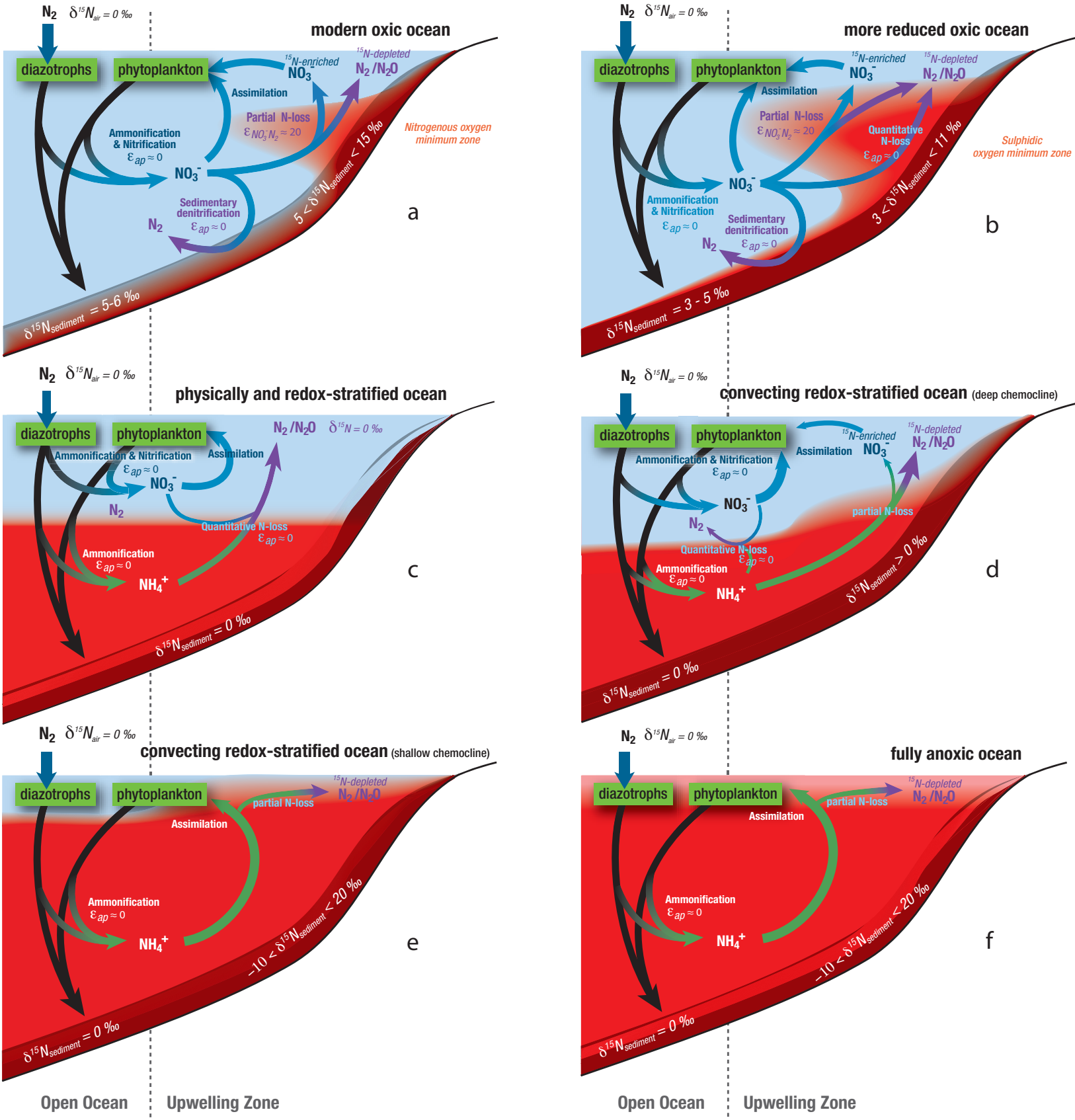
modern oxic ocean
more reduced oxic ocean
physically and redox-stratified ocean
convecting redox-stratified ocean (deep chemocline)
convecting redox-stratified ocean (shallow chemocline)
fully anoxic ocean
diazotrophs
phytoplankton
Assimilation
Partial N-loss
Ammonification & Nitrification
Sedimentary denitrification
Quantitative N-loss
Ammonification
partial N-loss
Nitrogenous oxygen minimum zone
Sulphidic oxygen minimum zone
a
b
c
d
e
f
Open Ocean
Upwelling Zone

Figure

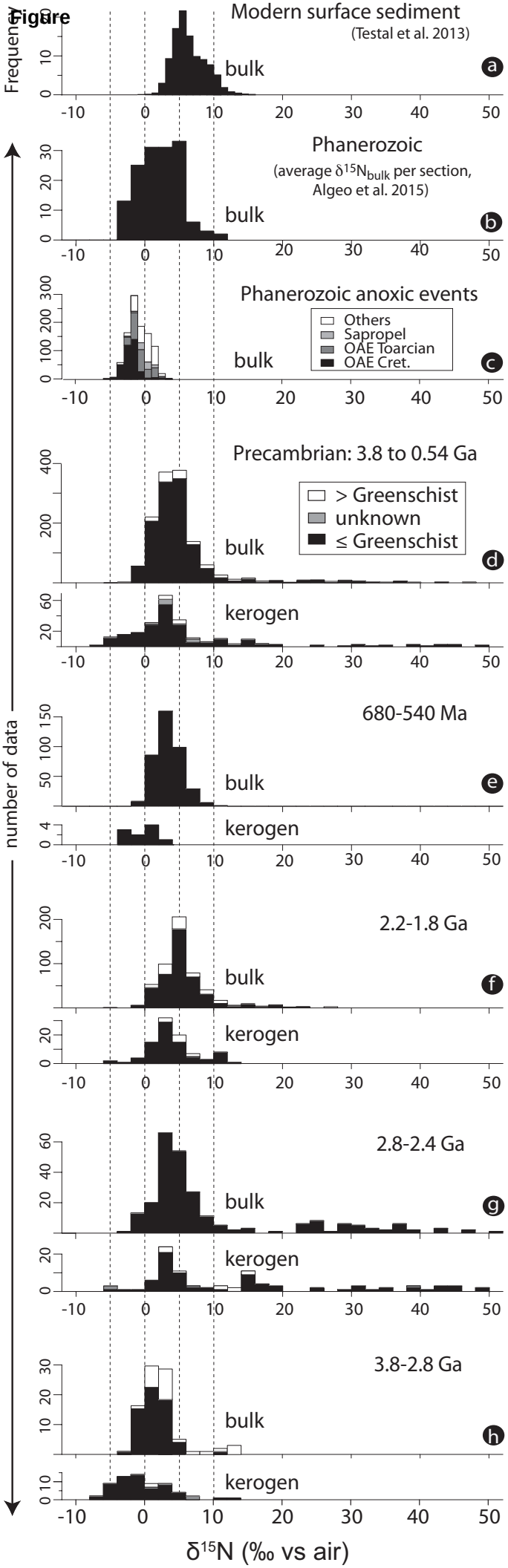
Frequency
number of data
Modern surface sediment
(Testal et al. 2013)
bulk
a
Phanerozoic
(average $\delta^{15}N_{bulk}$ per section,
Algeo et al. 2015)
bulk
b
Phanerozoic anoxic events
Others
Sapropel
OAE Toarcian
OAE Cret.
bulk
c
Precambrian: 3.8 to 0.54 Ga
> Greenschist
unknown
≤ Greenschist
bulk
kerogen
d
680-540 Ma
bulk
kerogen
e
2.2-1.8 Ga
bulk
kerogen
f
2.8-2.4 Ga
bulk
kerogen
g
3.8-2.8 Ga
bulk
kerogen
h
δ15N (‰ vs air)

Figure

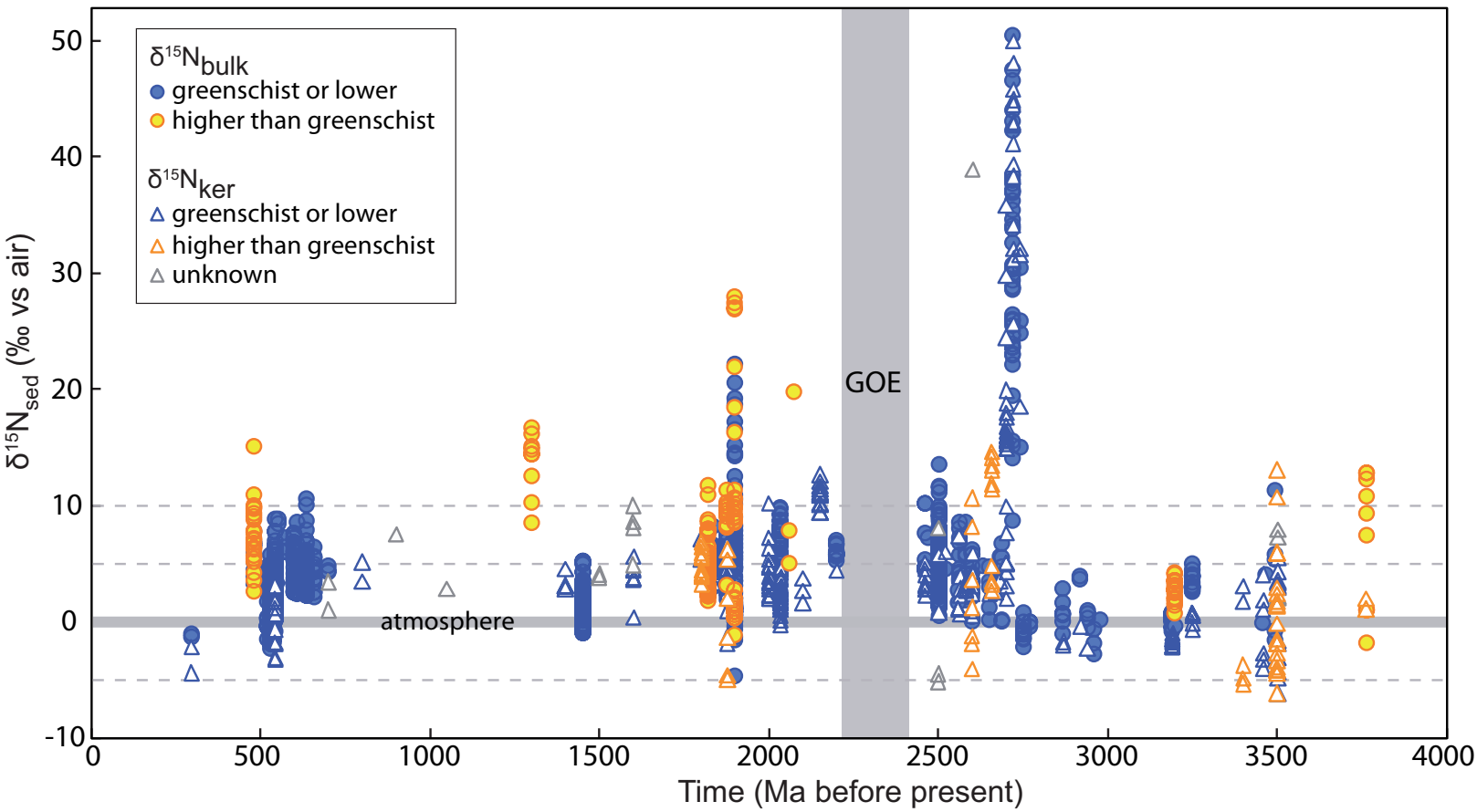
δ15Nbulk
greenschist or lower
higher than greenschist
δ15Nker
greenschist or lower
higher than greenschist
unknown
GOE
atmosphere
δ15Nsed (‰ vs air)
Time (Ma before present)
50
40
30
20
10
0
-10
0
500
1000
1500
2000
2500
3000
3500
4000

Background dataset for online publication only

Click here to download Background dataset for online publication only: Supplementary Compilation Precambrian d15Nsed revis

Background dataset for online publication only

Click here to download Background dataset for online publication only: supplementary references.doc